Lewis-Acid Properties of Technetium(VII) Dioxide Trifluoride, TcO_2F_3: Characterization by ^{19}F, ^{17}O, and ^{99}Tc NMR Spectroscopy and Raman Spectroscopy, Density Functional Theory Calculations of TcO_2F_3, $M^+TcO_2F_4^-$ [M = Li, Cs, $N(CH_3)_4$], and $TcO_2F_3{\cdot}CH_3CN$, and X-ray Crystal Structure of $Li^+TcO_2F_4^-$ †

William J. Casteel, Jr.,[1] David A. Dixon,[2] Nicolas LeBlond,[1] Hélène P. A. Mercier,[1] and Gary J. Schrobilgen*,[1]

Department of Chemistry, McMaster University, Hamilton, Ontario L8S 4M1, Canada, and William R. Wiley Environmental Molecular Sciences Laboratory, Pacific Northwest National Laboratory, 906 Battelle Blvd., P.O. Box 999, KI-83, Richland, Washington 99352

Received July 18, 1997

Technetium(VII) dioxide trifluoride, TcO_2F_3, behaves as a Lewis acid toward the fluoride ion and acetonitrile forming $M^+TcO_2F_4^-$ [M = Li, Cs, $N(CH_3)_4$] salts and $TcO_2F_3{\cdot}CH_3CN$. Fluorine-19 NMR spectroscopy established that the $TcO_2F_4^-$ anion has a *cis*-dioxo geometry in CH_3CN solution. Variable-temperature ^{19}F NMR studies of $TcO_2F_4^-$ and $TcO_2F_3{\cdot}CH_3CN$ in CH_3CN revealed that the one-bond couplings between ^{99}Tc and the two fluorine environments exhibit widely different degrees of quadrupolar collapse. The ^{17}O NMR spectra of ^{17}O-enriched $TcO_2F_4^-$ and $TcO_2F_3{\cdot}CH_3CN$ and the ^1H and ^{13}C NMR spectra of $TcO_2F_3{\cdot}CH_3CN$ indicated that chemical exchange occurs between $TcO_2F_3{\cdot}CH_3CN$ and CH_3CN solvent. The $TcO_2F_4^-$ anion was characterized by X-ray crystallography as its lithium salt crystallizing in the tetragonal system, space group $P\bar{4}2_1m$, with $a = 4.706(1)$ Å, $c = 8.797(2)$ Å, $V = 194.8(1)$ Å^3, and $Z = 2$, at 20 °C. Refinement converged with $R = 0.0339$ ($R_w = 0.0320$). The anion geometry is a distorted octahedron with the two oxygen ligands *cis* to each other and is closely related to the $[TcO_2F_4]$ units in polymeric TcO_2F_3. The Raman spectra of $M^+TcO_2F_4^-$ [M = Li, Cs, $N(CH_3)_4$] and $TcO_2F_3{\cdot}CH_3CN$ were assigned under C_{2v} and C_s point symmetries, respectively. Density functional theory calculations at the local and nonlocal levels predict that monomeric TcO_2F_3 has a trigonal bipyramidal geometry (C_{2v} point symmetry) and confirm that the *cis*-dioxo isomers of $TcO_2F_4^-$ and $TcO_2F_3{\cdot}CH_3CN$ (CH_3CN bonded *trans* to an oxygen) are the energy-minimized structures.

Introduction

Pertechnyl fluoride, TcO_3F, the first technetium(VII) oxide fluoride to be reported and unambiguously characterized, was prepared by Selig and Malm[3] by passing fluorine over TcO_2 in a nickel tube at 150 °C. Selig and co-workers[4] also characterized TcO_3F by vibrational spectroscopy and determined that TcO_3F can be prepared by solvolysis of TcO_4^- in anhydrous HF. It was later shown that TcO_3F can also be synthesized by solvolysis of the neutral oxide Tc_2O_7 in anhydrous HF.[5] Addition of XeF_6 to these solutions scavenges water produced in the solvolysis and fluorinates TcO_3F to give bright yellow TcO_2F_3, the second technetium(VII) oxide fluoride to have been characterized; technetium dioxide trifluoride was shown by X-ray crystallography and Raman spectroscopy to consist of open chains of fluorine-bridged $[TcO_2F_4]$ units in which the bridging fluorine atoms are *trans* to the oxygen atoms and the oxygen atoms are *cis* to one another.[5] The *cis*-dioxo arrangement has been observed in all other six coordinate d^0 transition metal dioxofluorides (e.g., OsO_2F_4,[6,7] $Os_2O_4F_7^+$,[8] $ReO_2F_4^-$,[9−11] $Re_2O_4F_7^-$,[9] $Re_3O_6F_{10}^-$,[9] $WO_2F_3^-$,[12] $WO_2F_4^{2-}$,[13,14] $MoO_2F_3^-$,[12] $MoO_2F_4^{2-}$,[15−17] $VO_2F_3^{2-}$,[18] and $VO_2F_4^{3-}$ [19]).

Fluorine bridging in the solid-state structure of TcO_2F_3

† Dedicated to Professor Neil Bartlett on the occasion of his 65th birthday.

(1) McMaster University.
(2) Pacific Northwest Laboratory.
(3) Selig, H.; Malm, J. G. *J. Inorg. Nucl. Chem.* **1963**, *25*, 349.
(4) Binenboym, J.; El-Gad, U.; Selig, H. *Inorg. Chem.* **1974**, *13*, 319.
(5) Mercier, H. P. A.; Schrobilgen, G. J. *Inorg. Chem.* **1993**, *32*, 145.
(6) Christe, K. O.; Bougon, R. J. *J. Chem. Soc., Chem. Commun.* **1992**, 1056.
(7) Christe, K. O.; Dixon, D. A.; Mack, H. G.; Oberhammer, H.; Pagelot, A.; Sanders, J. C. P.; Schrobilgen, G. J. *J. Am. Chem. Soc.* **1993**, *115*, 11279.
(8) Casteel, W. J., Jr.; Dixon, D. A.; Mercier, H. P. A.; Schrobilgen, G. J. *Inorg. Chem.* **1996**, *35*, 4310.
(9) Casteel, W. J., Jr.; Dixon, D. A.; LeBlond, N.; Lock, P. E.; Mercier, H. P. A.; Schrobilgen, G. J. *Inorg. Chem.*, to be submitted for publication.
(10) Kuhlmann, W.; Sawodny, W. *J. Fluorine Chem.* **1977**, *9*, 341.
(11) Bol'shakov, A. M.; Glushkova, M. A.; Buslaev, Y. A. *Dokl. Chem. (Engl. Transl.)* **1983**, *273*, 417; *Dokl. Akad. Nauk SSSR*, **1983**, *273*, 1134.
(12) Mattes, R.; Müller, G.; Becher, H. J. *Z. Anorg. Allg. Chem.* **1972**, *389*, 177.
(13) (a) Vlasse, M.; Moutou, J. M.; Cervera-Marzal, M.; Chaminade, J. P.; Hagenmuller, P. *Rev. Chim. Miner.* **1982**, *19*, 58. (b) Chaminade, J. P.; Moutou, J. M.; Villeneuve, G.; Couzi, M.; Pouchard, M.; Hagenmuller, P. *J. Solid State Chem.* **1986**, *65*, 27.
(14) Buslaev, Y. A.; Petrosyants, S. P. *J. Struct. Chem. (Engl. Transl.)* **1969**, *10*, 983; *Zh. Strukt. Khim.* **1969**, *10*, 1105.
(15) (a) Buslaev, Y. A.; Shcherbakov, V. A. *J. Struct. Chem. (Engl. Transl.)* **1966**, *7*, 332; *Zh. Strukt. Khim.* **1966**, *7*, 345. (b) Buslaev, Y. A.; Petrosyants, S. P.; Tarasov, V. P. *J. Struct. Chem. (Engl. Transl.)* **1970**, *11*, 574; *Zh. Strukt. Khim.* **1970**, *11*, 616. (c) Buslaev, Y. A.; Petrosyants, S. P.; Tarasov, V. P. *Dokl. Phys. Chem. (Engl. Transl.)* **1970**, *193*, 548; *Dokl. Akad. Nauk SSSR*, **1970**, *193*, 611.
(16) Sergienko, V. S.; Porai-Koshits, M. A.; Khodashova, T. S. *J. Struct. Chem. (Engl. Transl.)* **1972**, *13*, 431; *Zh. Strukt. Khim.* **1972**, *13*, 461.
(17) Grandjean, D.; Weiss, R. *Bull. Soc. Chim. Fr.* **1967**, *36*, 3049.

S0020-1669(97)00893-8 CCC: $15.00
Published on Web 01/01/1998

indicates that the TcO_2F_3 monomer should behave as a Lewis acid and possess a significant fluoride ion affinity. It has been shown by ^{19}F, ^{99}Tc, and ^{129}Xe NMR spectroscopy that excess XeF_6 reacts with Tc_2O_7 in HF (molar ratio of XeF_6:Tc_2O_7 = 5:1) to form stable solutions of $XeF_5^+TcO_2F_4^-$.[5] In the present work, the Lewis acid properties of TcO_2F_3 toward F^- and CH_3CN were investigated in detail, resulting in the full structural characterization of the $TcO_2F_4^-$ anion and $TcO_2F_3{\cdot}CH_3CN$.

Results and Discussion

Syntheses of $TcO_2F_4^-$ Salts and $TcO_2F_3{\cdot}CH_3CN$. Technetium dioxide trifluoride, TcO_2F_3, is essentially insoluble in anhydrous HF at room temperature but readily reacts with HF solutions of LiF, CsF, and $N(CH_3)_4F$ in 1:1 molar ratios to form orange, room temperature stable $M^+TcO_2F_4^-$ salts. The solubilities of the Cs^+ and $N(CH_3)_4^+$ salts in anhydrous HF are low when a large excess of solvent is present but increase significantly when the proportion of salt is high. This can be attributed to the comparable Lewis acidities of TcO_2F_3 and HF which compete for the strong Lewis bases CsF and $N(CH_3)_4F$ forming insoluble TcO_2F_3 and $(HF)_xF^-$ in solution. Because LiF is a weaker Lewis base, $Li^+TcO_2F_4^-$ is moderately soluble in HF and a suitable candidate for single crystal growth.

The Lewis acid properties of TcO_2F_3 are also observed when it is dissolved in CH_3CN and account for the high solubility of the polymeric solid in that solvent (eq 1). When the solvent

$$TcO_2F_3 + CH_3CN \xrightarrow{CH_3CN} TcO_2F_3{\cdot}CH_3CN \qquad (1)$$

was removed at −40 °C, a pale orange adduct, $TcO_2F_3{\cdot}CH_3CN$, remained, which slowly decomposed at room temperature under nitrogen to the starting materials, as determined by Raman spectroscopy.

Characterization of $TcO_2F_4^-$ and $TcO_2F_3{\cdot}CH_3CN$ by ^{19}F, ^{99}Tc, and ^{17}O NMR Spectroscopy. The magnetic properties of the ^{99}Tc nucleus make it an excellent NMR nuclide.[20] Although ^{99}Tc possesses an appreciable quadrupole moment ($Q = -129(6) \times 10^{-31}$ m^2),[21] the effect of quadrupole line broadening is attenuated by the large size of its nuclear spin ($I = {}^9/_2$). The low natural abundance of ^{17}O ($I = {}^5/_2$; 0.037%) required the use of ^{17}O-enriched samples (35.01% ^{16}O, 21.87% ^{17}O, 43.12% ^{18}O) in order to acquire ^{17}O NMR spectra in a reasonable amount of time.

$N(CH_3)_4^+TcO_2F_4^-$. The ^{19}F NMR spectrum of $N(CH_3)_4^+TcO_2F_4^-$ dissolved in CH_3CN at 30 °C consists of a well-resolved 1:2:1 triplet at −14.1 ppm ($\Delta\nu_{1/2}$ = 50 Hz) and a broad saddle-shaped feature at −18.7 ppm ($\Delta\nu_{1/2}$ = 1550 Hz), the two components having equal relative intensities (Figure 1a). The observation of two fluorine environments establishes the *cis*-geometry adopted by the oxygen ligands in $TcO_2F_4^-$ (structure **I**). The saddle-shaped feature results from spin coupling of the fluorine environment to the ^{99}Tc nucleus, yielding a partly quadrupole collapsed decet of 1:2:1 triplets.

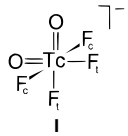

I

The triplet in the ^{19}F NMR spectrum arises from the two-bond coupling $^2J(^{19}F_c-^{19}F_t)$ = 105 Hz (the subscripts denote fluorines *trans* (t) to and *cis* (c) to the oxygen ligands, respectively). Interestingly, the scalar coupling to ^{99}Tc for this resonance is completely quadrupole collapsed. The assignments of the two signals were based on the relative magnitudes of their one-bond couplings with ^{99}Tc. The Tc−F_t bonds are weaker and longer (see X-ray Crystal Structure of $Li^+TcO_2F_4^-$) owing to the *trans*-influence of the strongly π-bonded oxygen ligands to the metal $d_{t_{2g}}$ orbitals, so that $^1J(^{99}Tc-^{19}F_t)$ is expected to be less than $^1J(^{99}Tc-^{19}F_c)$. The triplet at −14.1 ppm shows only slight line broadening arising from scalar coupling to ^{99}Tc whereas the broad saddle-shaped feature at −18.7 ppm clearly indicates scalar coupling to ^{99}Tc, leading to the assignment of the former resonance to F_t and the latter to F_c. These assignments are supported by a previous ^{19}F NMR study of $WO_2F_4^{2-}$ for which $^1J(^{183}W-^{19}F_c)$ = 118.0 Hz is significantly larger than $^1J(^{183}W-^{19}F_t)$ = 50.0 Hz.[14] The assignment of the two fluorine signals in $WO_2F_4^{2-}$ was confirmed by a variable-temperature ^{19}F NMR experiment in which selective broadening of the more weakly bonded F_t resonance arising from fluoride ion/solvent exchange was observed at elevated temperature. A similar experiment was performed with $TcO_2F_4^-$ in HF solvent and confirmed the ^{19}F assignments. The ^{19}F NMR spectrum of $Cs^+TcO_2F_4^-$ at 28 °C consists of only the *cis*-fluorine resonance at 23.0 ppm which showed partly collapsed scalar coupling to the ^{99}Tc nucleus (Figure 1b). No resonance corresponding to the *trans*-fluorine environment was observed, even when the spectrum was recorded at −80 °C, indicating rapid exchange of the more labile *trans*-fluorine with the solvent. Increasing the basicity of the solvent by addition of 30% and 5-fold molar excesses of CsF did not slow the exchange sufficiently at −80 °C to observe the *trans*-fluorine resonance. The *trans*-fluorine triplet of $ReO_2F_4^-$ was observed[9] for a CsF:ReO_2F_3 molar ratio of 5:1 at −80 °C and is consistent with the anticipated stronger Lewis acidity of ReO_2F_3 when compared to that of TcO_2F_3.

The ^{19}F NMR spectrum of $N(CH_3)_4^+TcO_2F_4^-$ in CH_3CN appears to be the only example, other than $TcO_2F_3{\cdot}CH_3CN$ (*vide infra*), in which a spin-${}^1/_2$ nucleus in two different chemical environments directly coupled to the same quadrupolar nucleus exhibits a large difference in their degree of quadrupolar collapse. This difference arises from the relationship between the spin−lattice relaxation rate of the quadrupolar nucleus (T_1^{-1}) and the $^1J(^{99}Tc-^{19}F)$ coupling constant. For the *trans*-fluorine resonance, the coupling constant is small relative to the relaxation rate of ^{99}Tc, i.e., $2\pi^1J(^{19}F_t-^{99}Tc) \ll T_1^{-1}$, leading to the observation of essentially complete quadrupole collapse of the scalar coupling. On the other hand, the larger scalar coupling between the ^{99}Tc nucleus and $^{19}F_c$ leads to a resonance that is only partly quadrupole collapsed, i.e., $2\pi^1J(^{19}F_c-^{99}Tc) \approx T_1^{-1}$. The spin−lattice relaxation time, determined from an inversion−recovery experiment, for ^{99}Tc in $N(CH_3)_4^+TcO_2F_4^-$ is 1.03 ms at 30 °C. This confirmed the assignments in the ^{19}F NMR spectrum since, according to the previous inequalities, a $^1J(^{99}Tc-^{19}F)$ significantly larger than $(2\pi{\cdot}1.03\ \text{ms})^{-1}$ = 155 Hz, as for $^1J(^{99}Tc-^{19}F_c)$ = 235 Hz (CH_3CN) and 260 Hz (HF) (*vide infra*), would result in a significantly quadrupole broadened fluorine resonance while a $^1J(^{99}Tc-^{19}F)$ smaller than 155 Hz

(18) Ryan, R. R.; Martin, S. H.; Reisfeld, M. J. *Acta Crystallogr., Sect. B* **1971**, *27*, 1270.
(19) Leimkühler, M.; Mattes, R. *J. Solid State Chem.* **1986**, *65*, 260.
(20) Rehder, D. In *Multinuclear NMR*; Mason, J., Ed.; Plenum Press: New York, 1987; pp 511−512.
(21) Raghavan, P. *At. Data Nuc. Data Tables* **1989**, *42*, 189.
(22) (a) Mason, J. In *Multinuclear NMR*; Mason, J., Ed.; Plenum Press: New York, 1987; Chapter 2. (b) Sanders J. C. P.; Schrobilgen, G. J. In *A Methodological Approach to Multinuclear NMR in Liquids and Solids-Chemical Applications*; NATO Advanced Study Institute, Magnetic Resonance; Granger, P., Harris, R. K. Eds.; Kluwer Academic Publishers: Dordrecht, The Netherlands, 1990; Chapter 11.

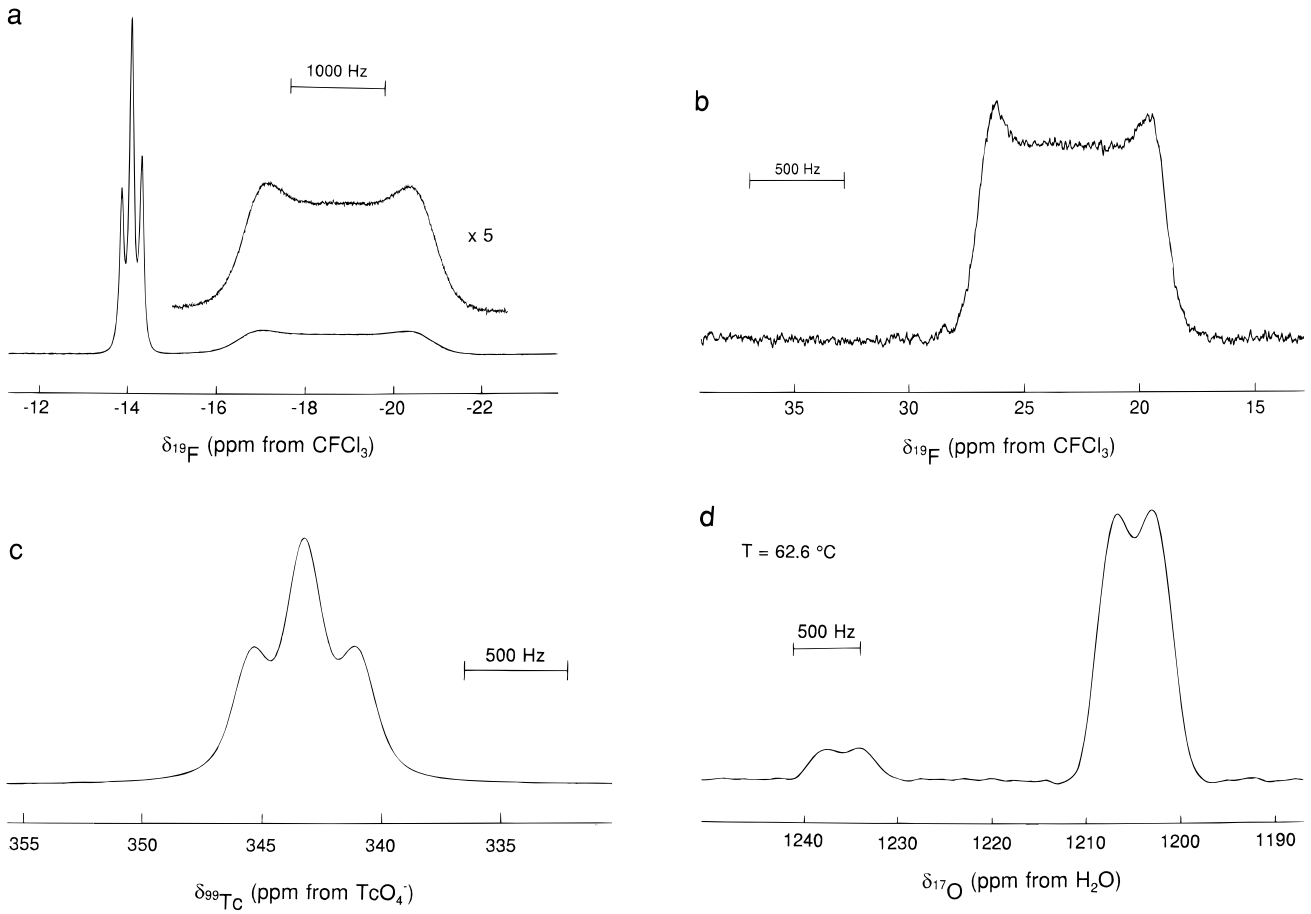

Figure 1. NMR spectra of $TcO_2F_4^-$: (a) ^{19}F (470.600 MHz), $N(CH_3)_4^+$ salt in CH_3CN solvent recorded at 30 °C; (b) ^{19}F (470.600 MHz), Cs^+ salt in HF solvent recorded at 30 °C; (c) ^{99}Tc (112.570 MHz), $N(CH_3)_4^+$ salt in CH_3CN recorded at 45 °C; (d) ^{17}O (67.801 MHz), $N(CH_3)_4^+$ salt in CH_3CN recorded at 63 °C (21.87% ^{17}O).

would show a significantly smaller increase in the line width of the fluorine resonance.

The ^{99}Tc NMR spectrum of $N(CH_3)_4^+TcO_2F_4^-$ dissolved in CH_3CN at 45 °C (Figure 1c) displays a broadened 1:2:1 triplet at 343.2 ppm having a coupling constant of 235 Hz (measured after Gaussian multiplication of the free induction decay, unresolved otherwise) arising from $^1J(^{99}Tc-^{19}F_c)$, and as in the ^{19}F spectrum, the $^1J(^{99}Tc-^{19}F_t)$ coupling was not resolved.[23] The ^{99}Tc NMR spectrum of $Cs^+TcO_2F_4^-$ in HF at 30 °C consists of a well resolved triplet at 247.4 ppm, with a coupling constant of 260 Hz. These results agree well with recently reported[5] values for $XeF_5^+TcO_2F_4^-$ in HF [$\delta(^{99}Tc) = 240.0$ ppm; $^1J(^{99}Tc-^{19}F_c) = 259$ Hz], and it is now clear that in an earlier multi-NMR study,[24] a triplet resulting from the reaction of $K^+TcO_4^-$ with excess XeF_6 or KrF_2 in HF at $\delta(^{99}Tc) = 245.9$ ppm [$^1J(^{99}Tc-^{19}F_c) = 259$ Hz] and tentatively assigned to $Tc_2O_5F_4$, in fact, arose from the $TcO_2F_4^-$ anion.

The ^{17}O NMR spectrum of $N(CH_3)_4^+TcO_2F_4^-$ dissolved in CH_3CN at 30 and 63 °C consists of a single resonance which displays a partly quadrupole collapsed multiplet arising from scalar coupling to ^{99}Tc at 1204 ppm ($\Delta\nu_{1/2} = 570$ Hz at 30 °C, 600 Hz at 63 °C) (Figure 1d).[25] The two-bond coupling between ^{17}O and either ^{19}F environment could not be resolved.

$TcO_2F_3 \cdot CH_3CN$. The high solubility of TcO_2F_3 in CH_3CN down to the melting point of the solvent (−45.7 °C) is attributed to complex formation. The ^{19}F NMR spectra of TcO_2F_3 in CH_3CN recorded at −40, 30, and 51 °C display two fluorine resonances (Figure 2). The spectrum at −40 °C shows a binomial triplet at 29.8 ppm ($\Delta\nu_{1/2} = 29$ Hz) and a broad resonance at 23.9 ppm ($\Delta\nu_{1/2} = 460$ Hz) having relative intensities of 1:2. Although it was not possible to determine the relative positions of the oxygen atoms from this spectrum, a *cis*-dioxo arrangement (structure **II**) is assumed on the basis

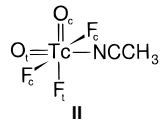

II

of the experimental structures of $TcO_2F_4^-$, TcO_2F_3,[5] and all other d^0 transition metal dioxide fluorides as well as the energy minimized structures determined by local density functional theory (LDFT) (see Computational Results). Furthermore, the CH_3CN coordinates *trans* to the oxygen atom in its complexes with WOF_4,[26] $MoOF_4$,[27] and VOF_4^-,[28] rendering all fluorine atoms equivalent in their ^{19}F NMR spectra. Consequently, the

(23) A weak resonance at 304.0 ppm was also observed and is tentatively assigned to the dinuclear anion $Tc_2O_4F_7^-$.
(24) Franklin, K. J.; Lock, C. J. L.; Sayer, B. G.; Schrobilgen, G. J. *J. Am. Chem. Soc.* **1982**, *104*, 5303.
(25) A weak resonance at 1235 ppm was also observed and is tentatively assigned to the dinuclear anion $Tc_2O_4F_7^-$.
(26) Buslaev, Y. A.; Kokunov, Y. V.; Bochkareva, V. A. *J. Struct. Chem. (Engl. Transl.)* **1972**, *13*, 570; *Zh. Strukt. Khim.* **1972**, *13*, 611.
(27) Buslaev, Y. A.; Kokunov, Y. V.; Bochkaryova, V. A.; Shustorovich, E. M. *J. Inorg. Nucl. Chem.* **1972**, *34*, 2861.
(28) Hibbert, R. C. *J. Chem. Soc., Chem. Commun.* **1985**, 317.

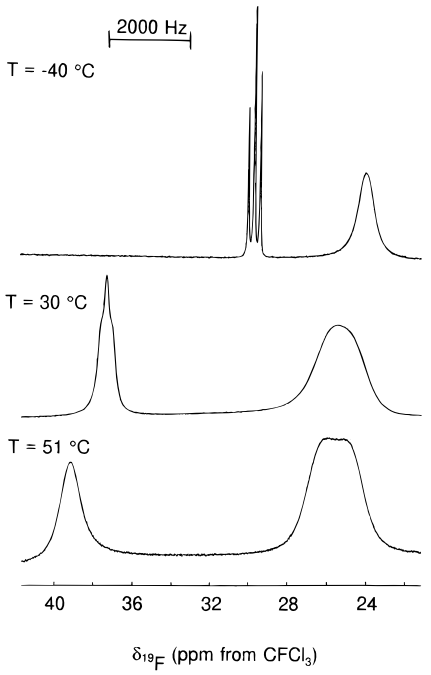

Figure 2. Variable-temperature ^{19}F NMR spectra (470.600 MHz) of TcO_2F_3 (0.36 M) dissolved in CH_3CN.

Scheme 1

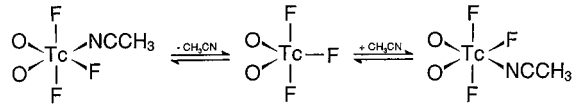

triplet of the $TcO_2F_3{\cdot}CH_3CN$ adduct is reasonably assigned to the fluorine atom *trans* to an oxygen ligand with a two-bond spin−spin coupling to the *cis*-fluorine atoms, $^2J(^{19}F_c-^{19}F_t) = 147$ Hz. This fluorine environment is only very weakly coupled to the ^{99}Tc nucleus owing to the *trans*-influence of the oxygen ligands (*vide supra*) as noted for $TcO_2F_4^-$. The signal assigned to the *cis*-fluorine atoms appears at 23.9 ppm, is broadened by partly quadrupole-collapsed spin coupling to ^{99}Tc, and is analogous to what was observed for the $TcO_2F_4^-$ anion. The relative order of the chemical shifts for the two fluorine environments is opposite to that observed for $ReO_2F_3{\cdot}CH_3CN$ (triplet, −24.5 ppm, and doublet, −31.3 ppm).[9] At higher temperatures, the *trans*-fluorine resonance of $TcO_2F_3{\cdot}CH_3CN$ is shifted to higher frequency (37.3 ppm at 30 °C; 39.2 ppm at 51 °C) relative to that of the *cis*-fluorine resonance (25.3 ppm at 30 °C; 25.8 ppm at 51 °C). The larger deshielding of the *trans*-fluorine resonance could result from an exchange process between the CH_3CN ligand and the solvent by means of a trigonal bipyramidal TcO_2F_3 intermediate (Scheme 1). Under these conditions, intramolecular exchange of the two fluorine environments would be restricted because of the large energy barrier associated with having the oxo ligands of the TcO_2F_3 intermediate in axial positions (see Computational Results). The increased line widths of the *cis*- and *trans*-fluorine resonances with increasing temperature result from decreases in the relaxation rate of ^{99}Tc as the molecular correlation time decreases at higher temperature. At −40 °C, $^1J(^{19}F_t-^{99}Tc)$ spin-coupling is not observed because of the fast relaxation rate of the ^{99}Tc nucleus relative to the $^1J(^{19}F_t-^{99}Tc)$ coupling constant, i.e., $1/T_1(^{99}Tc) \gg 2\pi^1J(^{99}Tc-^{19}F_t)$.[22] At 30 and 51 °C, the rate of quadrupole relaxation is slower and results in significant broadening of the triplet. A similar effect is observed for the *cis*-fluorine resonance which is a broad singlet at −40 °C that evolves into a "flat-topped" unresolved multiplet (an unresolved doublet of equi-intense decets) at 51 °C.

Table 1. Summary of Crystal Data and Refinement Results for $Li^+TcO_2F_4^-$

empirical formula	F_4LiO_2Tc
space group	$P42_1m$ (No. 113)
a (Å)	4.706(1)
c (Å)	8.797(2)
V (Å^3)	194.8(1)
molecules/unit cell	2
molecular wt (g mol^{-1})	212.94
calcd density (g cm^{-3})	3.63
T (°C)	22
color	orange
μ (cm^{-1})	36.89
wavelength (Å) used for data collcn	0.56086
final agreement factors	$R^a = 0.0339$
	$R_w{}^b = 0.0320$

$^a R = \sum||F_o| - |F_c||/\sum|F_o|$. $^b R_w = [\sum[w(|F_o| - |F_c|)^2]/\sum w(|F_o|)^2]^{1/2}$, where $w = 1/[\sigma^2(F) + 0.0006F^2]$.

Ligand exchange between TcO_2F_3 and CH_3CN solvent was investigated by variable-temperature ^1H, ^{13}C, and ^{19}F NMR spectroscopy for a 1:6 molar mixture of TcO_2F_3 and CH_3CN in SO_2ClF. The ^{19}F NMR spectrum recorded at −75 °C shows a sharp triplet at 32.2 ppm and a broad doublet at 25.9 ppm corresponding to the coupling constant $^2J(^{19}F_c-^{19}F_t) = 148$ Hz. In the ^1H NMR spectrum, the resonance attributed to complexed CH_3CN (2.16 ppm) was observed as a shoulder on the free CH_3CN resonance (1.79 ppm). Exchange with free CH_3CN occurs at higher temperatures, leading to the collapse of the ^1H resonances of complexed and free CH_3CN at −20 °C and slow decomposition above 0 °C. Complexation shifts in the ^{13}C NMR spectrum at −75 °C could not be resolved from the free CH_3CN resonances at 1.1 and 117.8 ppm because of line broadening arising from residual spin−spin coupling to the ^{99}Tc nucleus. Furthermore, the CH_3CN complexation shifts are expected to be smaller for the $TcO_2F_3{\cdot}CH_3CN$ adduct than for the $ReO_2F_3{\cdot}CH_3CN$ adduct because ReO_2F_3 is a stronger Lewis acid than TcO_2F_3 (complexation shifts observed for $ReO_2F_3{\cdot}CH_3CN$: ^1H, 0.46 ppm; ^{13}CN, 1.54 ppm; $^{13}CH_3$, 1.08 ppm).[9]

The ^{99}Tc NMR resonances of TcO_2F_3 recorded in CH_3CN at −41 and 30 °C are broad (265.3 ppm, $\Delta\nu_{1/2} = 4200$ Hz at −41 °C; 267.4 ppm, $\Delta\nu_{1/2} = 1650$ Hz at 30 °C), precluding observation of either $^1J(^{99}Tc-^{19}F_t)$ or $^1J(^{99}Tc-^{19}F_c)$ and indicate that the electric field gradient at the technetium nucleus in $TcO_2F_3{\cdot}CH_3CN$ is significantly greater than in $TcO_2F_4^-$.

The ^{17}O NMR spectra of TcO_2F_3 in CH_3CN recorded at −41 and 30 °C consist of a broad singlet (1205 ppm, $\Delta\nu_{1/2} = 264$ Hz at −41 °C; 1203 ppm, $\Delta\nu_{1/2} = 266$ Hz at 30 °C) which is significantly narrower than in $TcO_2F_4^-$ because of the faster relaxation rate of the ^{99}Tc nucleus in the more asymmetric ^{99}Tc environment of $TcO_2F_3{\cdot}CH_3CN$. Although theory predicts that the adduct has a *cis*-dioxo arrangement and that the two ^{17}O environments (O *trans* to F and O *trans* to CH_3CN) will differ by about 25 ppm (see Computational Results), only one resonance was detected in the ^{17}O NMR spectrum. The observation of a single resonance is consistent with ligand exchange behavior observed in the ^1H NMR spectrum. Moreover, the nearly identical ^{17}O chemical shifts in $TcO_2F_4^-$ and in $TcO_2F_3{\cdot}CH_3CN$ further support the assumption that the oxygen ligands retain their *cis* arrangement in the adduct.

X-ray Crystal Structure of $Li^+TcO_2F_4^-$. Details of the data collection parameters and other crystallographic information are given in Table 1. The final atomic coordinates and the

Table 2. Final Atomic Coordinates ($\times 10^4$) and Equivalent Isotropic Displacement Coefficients ($Å^2 \times 10^3$) in $Li^+TcO_2F_4^-$

	x	*y*	*z*	*U*(eq)[a]
Tc(1)	0	5000	2256(1)	13(1)
F(1)	2209(5)	−2791(5)	7450(5)	24(1)
F(2)	1851(4)	−3149(4)	4027(4)	20(1)
O(1)	−1945(6)	−6945(6)	1074(5)	25(1)
Li(1)	5000	0	4204(2)	25(2)

[a] Equivalent isotropic *U* defined as one-third of the trace of the orthogonalized $\mathbf{U}_{ij}$ tensor.

Table 3. Bond Lengths (Å), Bond Valences (vu), and Bond Angles (deg) in $Li^+TcO_2F_4^-$

Bond Lengths and Corresponding Bond Valences[a]

	Tc(1)−F(1)	Tc(1)−F(2)	Tc(1)−O(1)
bond valence	0.883	0.656	1.862
bond length	1.876(3)	1.986(3)	1.660(4)
tot. bond valence	6.80		
	Li(1)−F(1)	Li(1)−F(2)	Li(1)−F(2)′
bond valence	0.147	0.185	0.135
bond length	2.07(1)	1.99(1)	2.10(3)
tot. bond valence	0.93		

Bond Angles

O(1)−Tc(1)−O(1A)	102.5(3)	F(2)−Tc(1)−O(1)	90.4(2)
O(1)−Tc(1)−F(1)	94.9(1)	F(2)−Tc(1)−F(1)	83.8(1)
F(1)−Tc(1)−F(1A)	164.2(3)	F(2)−Tc(1)−F(2A)	76.7(2)
F(2)−Tc(1)−O(1A)	167.1(2)		

[a] Bond valence units (vu) are defined in ref 32. $R_0 = 1.89$ (Tc═O), $R_0 = 1.83$ (Tc−F), and $B = 0.37$ were used: Brown, I. D. Department of Physics, McMaster University, Hamilton, Ontario L8S 4M1, Canada, private communication.

equivalent thermal parameters are summarized in Table 2. Important bond lengths and angles and significant long contacts are listed in Table 3.

The structure of the $TcO_2F_4^-$ anion consists of a technetium atom bonded to two oxygen atoms that are *cis* to each other and *trans* to two fluorine atoms (F_t) and two fluorine atoms that are *cis* to oxygen (F_c) and *trans* to each other (Figure 3a). The distorted octahedral arrangement of the anion is closely related to the $[TcO_2F_4]$ units in polymeric TcO_2F_3 in which the *cis*-oxygen atoms are *trans* to the fluorine bridges.[5] The anion has long contacts with five neighboring cations through both the *cis*- and the *trans*-fluorine atoms (Figure 3b). The extended structure of the salt (Figure 4) consists of an infinite layer of cations sandwiched between two infinite layers of anions with the oxygen atoms forming the exterior faces of the anion layers. The structure of $TcO_2F_4^-$ is very similar to that of isoelectronic $ReO_2F_4^-$,[9] $WO_2F_4^{2-}$,[13] and $VO_2F_4^{3-}$,[19] which also adopt the *cis*-dioxo geometry and similar extended structures.

The Tc−O distance (1.660(4) Å) is characteristic of a Tc−O double bond. It is slightly longer than the Tc−O bond length found in TcO_2F_3 (1.646(9) Å),[5] slightly shorter than the Tc−O bond lengths found in Tc_2O_7 (1.672(8) Å, terminal),[29] $N(CH_3)_4^+TcO_4^-$ (1.676(8) Å),[30] and similar to that observed in the trimer $(TcOF_4)_3$ (1.66(3) Å),[31] where technetium is in its +6 oxidation state. The Tc−F_c bond length (1.876(3) Å) is longer than the terminal Tc−F bond distances in $(TcOF_4)_3$ (1.81(3) Å) and in TcO_2F_3 (1.834(7) Å), while the Tc−F_t bond

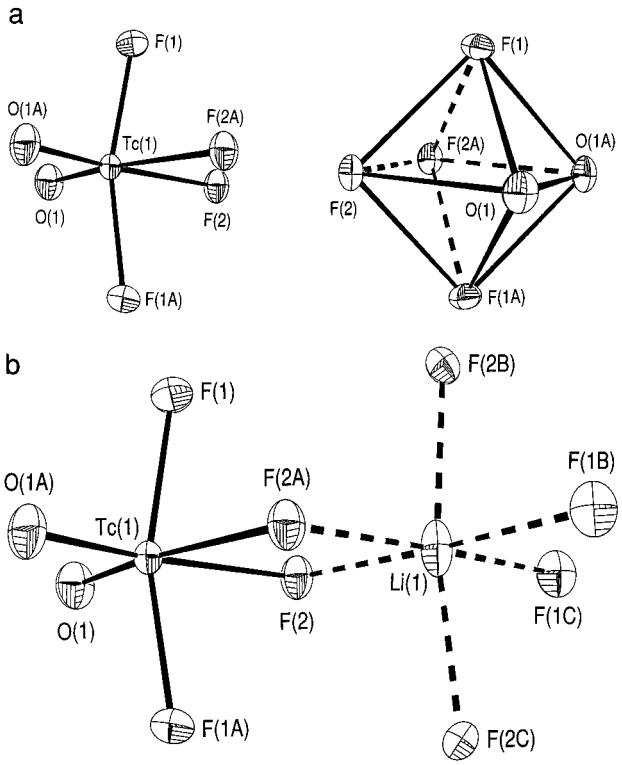

Figure 3. Structure of $Li^+TcO_2F_4^-$ showing thermal ellipsoids at the 50% probability level. (a) Geometry of the $TcO_2F_4^-$ anion and octahedron formed by the atoms around technetium in $TcO_2F_4^-$; (b) arrangement of the fluorine atoms around the Li^+ cation.

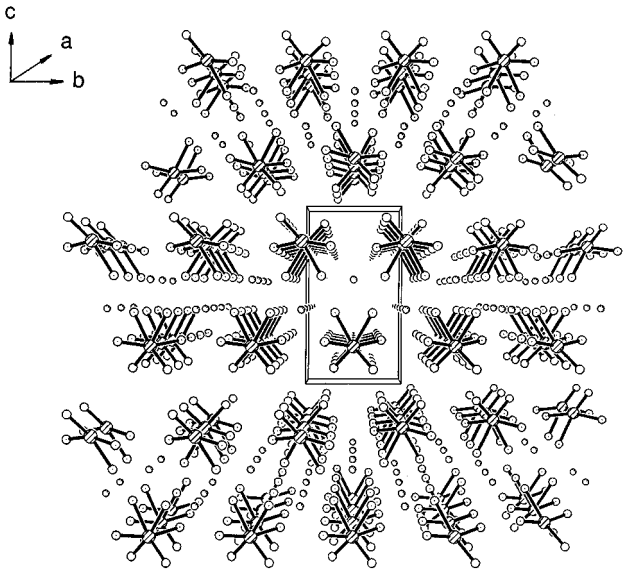

Figure 4. View of the $Li^+TcO_2F_4^-$ unit cell showing the packing along the *a*-axis.

(1.986(3) Å) is much longer and can only be compared to the Tc−F bridging bonds in TcO_2F_3 (average, 2.080(5) Å), which are also *trans* to oxygen atoms. These variations in the Tc−F and Tc−O bond lengths in $TcO_2F_4^-$ relative to the model compounds can be rationalized in terms of increased bond polarities anticipated because of the negative charge of the anion.

The bond valences for individual bonds, as defined by Brown,[32] are given in Table 3. The total bond valence for the technetium atom is 6.80 vu (bond valence units), with contributions of 1.86 vu/oxygen atom, 0.88 vu/*cis*-fluorine atom, and 0.66 vu/*trans*-fluorine atom. The values for the Tc−O double bond and Tc−F_c bond are lower than in TcO_2F_3 (1.97 and 0.99

(29) Krebs, B. *Z. Anorg. Allg. Chem.* **1971**, *380*, 146.
(30) German, K. E.; Grigor'ev, M. S.; Kuzina, A. F.; Gulev, B. F.; Spitsyn, V. I. *Dokl. Chem. (Engl. Transl.)* **1986**, *287*, 60; *Dokl. Akad. Nauk SSSR* **1986**, *287*, 650.
(31) Edwards, A. J.; Jones, G. R.; Sills, R. J. C. *J. Chem. Soc. A* **1970**, 2521.

vu, respectively) while the bond valence for the Tc−F_t bond is larger than for the bridging Tc−F bond in TcO_2F_3 (0.51 vu). Each Li^+ cation is coordinated to six fluorine atoms (Figure 3b), two of which are *trans*-fluorine atoms belonging to the same anion. Although the total bond valence sum for the lithium atom (0.93 vu) indicates it is slightly underbonded, the contributions of 0.15 vu/*cis*-fluorine atom and 0.18 and 0.13 vu/*trans*-fluorine atom account for the most significant contacts.

Despite considerable variations in the bond lengths and bond angles around the technetium atom in $TcO_2F_4^-$, the octahedron formed by the light atoms is relatively undistorted[33] having $F_c\cdots F_t$, $F_t\cdots F_t$, $F_c\cdots O$, $F_t\cdots O$, and $O\cdots O$ distances of 2.580(4), 2.466(6), 2.609(5), 2.600(6), and 2.587(8) Å, respectively. The VSEPR model of molecular geometry[34] provides a satisfactory explanation for the distortion observed for the coordination sphere of the technetium atom. The greater spatial requirements of the oxygen double bond domains and their repulsive interactions with single bond pair domains at approximately right angles to it in the [O, F_c, F_c, F_t] planes causes a bending of the F_c−Tc−F_c angle away from the oxygen atoms. This angle is 164.2(3)° in $Li^+TcO_2F_4^-$ and represents a significantly smaller deviation from the ideal 180° angle than is found in TcO_2F_3 (154.9(3)−155.9(3)°).[5] The difference is consistent with the more polar Tc−O and Tc−F bonds of $TcO_2F_4^-$, which is reflected in their smaller bond valence values and results in weaker bond pair−bond pair repulsions in $Li^+TcO_2F_4^-$ than in TcO_2F_3. These weaker bond-pair repulsions are also reflected in the large O−Tc−O angle (102.5(3)°) and the small F_t−Tc−F_t angle (76.7(2)°) and are presumably heightened by the smaller spatial requirements of the longer Tc−F_t bond domains.

Although the VSEPR model qualitatively accounts for the irregular octahedral geometry around the technetium, it does not account for the greater stability of the *cis*-arrangement of the oxygen atoms in its traditional form. The preference for the *cis*-dioxo structure can be understood in terms of the spatial relationship of the strong π-donor oxygen atoms to the approximately $d_{t_{2g}}$ orbitals of technetium required for p_π−d_π bonding. This type of arrangement has been observed for other transition metal oxide fluorides such as OsO_2F_4,[7] $ReO_2F_4^-$,[9−11] TcO_2F_3,[5] and MoO_2F_2·2thf (thf = tetrahydrofuran).[35] This p_π−d_π bonding effect is not observed for the $IO_2F_4^-$ anion, which occurs as a kinetically determined mixture of *cis*- and *trans*-isomers.[36] Recently, the geometries of non-VSEPR molecules have been explained in terms of core electron distortions.[37] In this model, the preference for the *cis*-dioxo arrangement in d^0 transition metal complexes is attributed to nonspherical metal atom cores resulting from the distortion produced by the ligands. Calculation of the Laplacian of the electron density in these molecules reveals the formation of local concentrations of electron density in the outer shell of the core so that the geometry of a molecule is determined by the tendency of the more covalently bonded ligands to occupy sites facing regions of local charge depletion. For the dioxo d^0 transition metal complexes it was determined that the oxygen ligands face larger depletions of charge in the *cis* isomer than in the *trans* isomer, rendering the *cis*-isomer more stable.

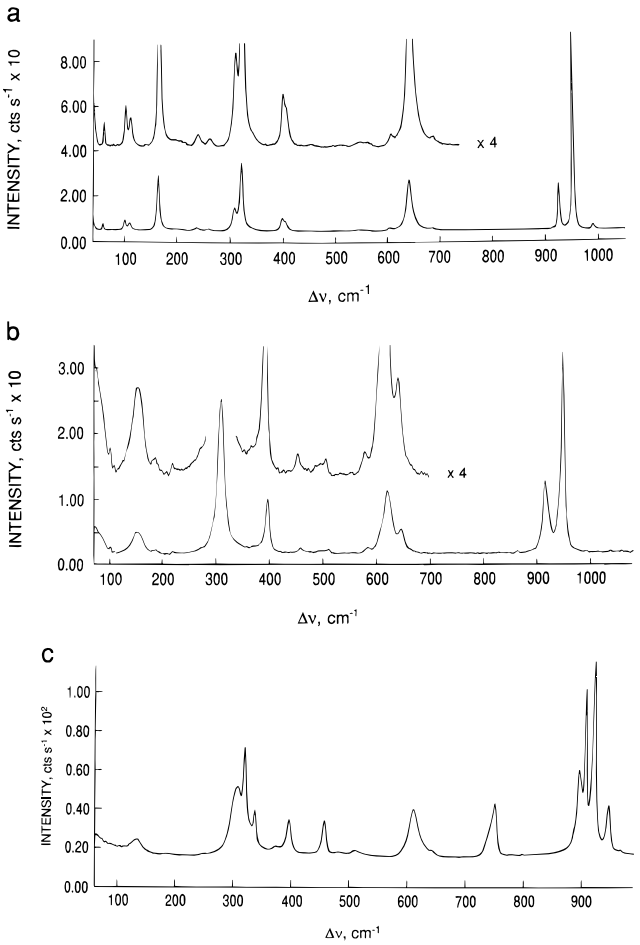

Figure 5. Raman spectra of microcrystalline (a) $Li^+TcO_2F_4^-$, (b) $Cs^+TcO_2F_4^-$, and (c) $N(CH_3)_4^+TcO_2F_4^-$ recorded in Pyrex capillaries at 20 °C using 647.1-nm excitation. The high-frequency bands of the $N(CH_3)_4^+$ cation are not shown but are listed in Table 4, footnote d.

Raman Spectroscopy and Vibrational Assignments for $M^+TcO_2F_4^-$ [M = Li, Cs, $N(CH_3)_4$] and TcO_2F_3·CH_3CN. The Raman spectra of the $TcO_2F_4^-$ salts are shown in Figure 5. The observed frequencies and their assignments for the *cis*-dioxo geometry of the $TcO_2F_4^-$ anion under the point group C_{2v} are listed in Table 4 (see X-ray Crystal Structure of $Li^+TcO_2F_4^-$).

All 15 vibrational modes having the symmetries $6A_1 + 2A_2 + 4B_1 + 3B_2$ (the [O, O, Tc, F_t, F_t]-plane is taken as the σ_v-(*xz*)-plane with *z* as the principal axis) are Raman active, and the A_1, B_1, and B_2 modes are infrared active. The vibrational assignments were made by comparison with the calculated frequencies (see Table 4 and Computational Results) and assignments for $ReO_2F_4^-$,[9,10] OsO_2F_4,[7] the $TcO_2F_4^-$ units of TcO_2F_3,[5] and the *cis*-isomer of $IO_2F_4^-$.[36]

The symmetry of the free $TcO_2F_4^-$ anion (C_{2v}), which happens to be identical to the site symmetry, was correlated to

(32) (a) Brown, I. D. *J. Solid State Chem.* **1974**, *11*, 214. (b) Brown, I. D. In *Structure and Bonding in Crystals*; O'Keefe, M., Navrotsky, A., Eds.; Academic Press: London, 1981; Vol. 2, p 1. (c) Brown, I. D.; Altermatt, D. *Acta Crystallogr.* **1985**, *B41*, 244.

(33) The eccentricities of the technetium atom in the octahedron defined by its ligand atoms are described relative to the three orthogonal planes of the octahedron. As noted earlier, the two oxygen atoms, their *trans*-fluorine atoms, and the technetium atom of the $TcO_2F_4^-$ anion are coplanar. The two [O, F_c, F_c, F_t] planes orthogonal to the [O, O, Tc, F_t, F_t] plane do not contain the technetium atom; consequently, the distortion of the octahedral environment around each technetium atom is described as a displacement of 0.191 Å of the technetium atom from both [O, F_c, F_c, F_t] planes toward the oxygen atoms in the [O, O, Tc, F_t, F_t] plane. This displacement is significantly less than that observed for the metal atoms in $MoOF_4$ (0.31 Å), WOF_4 (0.30 Å), $ReOF_4$ (0.30 Å), $TcOF_4$ (0.36 Å), and TcO_2F_3 (0.216−0.257 Å).

(34) Gillespie, R. J.; Hargittai, I. *The VSEPR Model of Molecular Geometry*; Allyn and Bacon: Boston, MA, 1991.

(35) Rhiel, M.; Wocadlo, S.; Massa, W.; Dehnicke, K. *Z. Anorg. Allg. Chem.* **1996**, *622*, 1195.

(36) Christe, K. O.; Wilson, R. D.; Schack, C. J. *Inorg. Chem.* **1981**, *20*, 2104.

(37) Gillespie, R. J.; Bytheway, I.; Tang, T. H.; Bader, R. F. *Inorg. Chem.* **1996**, *35*, 3954.

Table 4. Experimental Raman and Calculated Vibrational Frequencies, Assignments, and Mode Descriptions for $M^+TcO_2F_4^-$ [M = Li, Cs, $N(CH_3)_4$]

frequencies (cm^{-1})							
expt[a]			LDFT[b]		NLDFT[b]		
$LiTcO_2F_4$[d]	$CsTcO_2F_4$	$N(CH_3)_4TcO_2F_4$[e]	TZVP	DZVP	TZVP	DZVP	assgnts for $TcO_2F_4^-$ in C_{2v} pt sym[c]
954 (100)	950 (100)	922 (100), 907 (87)	935 (126)	921 (138)	893 (120)	881 (204)	$\nu_1(A_1)$, $\nu_{sym}(TcO_2)$
927 (23)	916 (32)	896 (44, sh)	935 (201)	983 (118)	890 (190)	883 (130)	$\nu_9(B_1)$, $\nu_{as}(TcO_2)$
641 (27)	649 (11)	643 (3)	638 (256)	645 (262)	590 (246)	598 (248)	$\nu_{13}(B_2)$, $\nu_{as}(TcF_{2c})$
605 (2)	623 (30)	612 (24)	628 (97)	630 (90)	582 (92)	582 (81)	$\nu_2(A_1)$, $\nu_{sym}(TcF_{2c} + TcF_{2t})$
553 (1), br	587 (3)	555 (4)	547 (31)	551 (27)	504 (30)	509 (29)	$\nu_3(A_1)$, $\nu_{sym}(TcF_{2c} - TcF_{2t})$
517 (<1)	515 (2)	512 (4)	527 (70)	532 (64)	486 (66)	489 (60)	$\nu_{10}(B_1)$, $\nu_{as}(TcF_{2t})$
453 (<1)	464 (2)	483 (2)					*f*
404 (5, sh), 399 (7)	402 (25)	398 (19)	372 (3)	369 (2)	370 (3)	363 (2)	$\nu_4(A_1)$, $\delta_{sciss}(TcO_2)$
320 (35)	315 (70)	338 (24), 320 (56)	317 (6)	307 (6)	303 (5)	293 (5)	$\nu_5(A_1)$, sym comb of *cis* and *trans* TcF_2 scissor
			306 (14)	302 (16)	302 (16)	297 (168)	$\nu_{14}(B_2)$, $\delta_{rock}(TcF_{2c})$
307 (12)	298 (12, sh)	309 (35, sh)	293 (21)	293 (20)	287 (22)	289 (19)	$\nu_{11}(B_1)$, sym comb of $OTcF_t$ sciss and TcF_{2c} sciss
			295 (0)	298 (0)	290 (0)	288 (0)	$\nu_7(A_2)$, TcO_2 torsion
259 (1)		249 (<1)					*f*
236 (2)	227 (2)	218 (<1)	236 (36)	235 (35)	234 (34)	233 (31)	$\nu_{15}(B_2)$, $\delta_{rock}(TcF_{2t})$
	194 (2)	184 (<1)	209 (1)	203 (1)	202 (1)	195 (1)	$\nu_6(A_1)$, antisym comb of *cis* and *trans* TcF_2 scissor
162 (29)	162 (10, br)	135 (7)	161 (0)	162 (0)	157 (0)	162 (0)	$\nu_{12}(B_1)$, antisym comb of $OTcF_t$ sciss and TcF_{2c} sciss
107 (3), 98 (5)	118 (1), 110 (1)						lattice modes
56 (3)			43 (0)	58 (0)	53 (0)	64(0)	$\nu_8(A_2)$, TcF_{2t} torsion

[a] Spectra recorded on microcrystalline powders in Pyrex glass melting point capillaries at room temperature using 647.1-nm excitation. Values in parentheses denote relative Raman intensities; sh = shoulder, and br = broad band. [b] Infrared intensities, in km mol^{-1}, are given in parentheses. [c] The fluorine atom labeling scheme is given by structure **I**. [d] Additional weak bands were observed for $Li^+TcO_2F_4^-$ at 991 (2) and 685 (2) cm^{-1}. [e] Frequencies observed for $N(CH_3)_4^+$: 364 (3) and 373 (5), $\nu_8(E)$; 457 (18), $\nu_{19}(T_2)$; 741 (12, sh), 752 (27), $\nu_3(A_1)$; 948 (26), $\nu_{18}(T_2)$; 1178 (3), $\nu_7(E)$; 1287 (2), $\nu_{17}(T_2)$; 1410 (2), 1418 (2), $\nu_{16}(T_2)$; 1462 (11), 1470 (10), $\nu_2(A_1)$; 2824 (3), 2879 (2), 2930 (4), 2964 (4), 2987 (4), 3032 (7), $\nu_5(E)$. [f] Unassigned bands.

the crystal symmetry (D_{2d}).[38] Only the A_1 bands ($\nu_1-\nu_6$) are expected to be factor-group split in the Raman spectrum whereas no bands are predicted to be split in the infrared spectrum. In fact, no factor-group splitting could be resolved on $\nu_1-\nu_6$ in the Raman spectrum of $Li^+TcO_2F_4^-$.

The symmetric and antisymmetric TcO_2 stretching modes [Li^+, 954 and 927 cm^{-1}; Cs^+, 950 and 916 cm^{-1}; $N(CH_3)_4^+$, 922, 907, and 896 cm^{-1}] appear at lower frequencies than the [TcO_2F_4] unit in the fluorine-bridged TcO_2F_3 structure (974 and 963, 958 cm^{-1}), which is expected for the more polar Tc−O bonds of the anion. The significant low-frequency shift in going from the Li^+ salt to the Cs^+ salt to the $N(CH_3)_4^+$ salt is attributed to progressive lowering of the Lewis acidity over the cation series, resulting in increasing negative charge on the $TcO_2F_4^-$ anion and increasing polarization of the Tc−O bonds. The bands at 641 (Li^+), 649 (Cs^+), and 643 cm^{-1} ($N(CH_3)_4^+$) are assigned to the antisymmetric Tc−F_c stretching mode and are slightly lower than in TcO_2F_3 (632, 650 cm^{-1}), which is consistent with the trend in bond valencies that these bonds exhibit in their respective crystal structures (0.88 vu in $Li^+TcO_2F_4^-$ and 0.95 to 1.05 vu in TcO_2F_3[5]). The Tc−F_t bond valence (0.66 vu) is significantly lower than that of Tc−F_c (1.04 vu) because of the *trans*-influence of the oxygen, so that the antisymmetric Tc−F_t stretching mode is found to occur at correspondingly lower frequency than the antisymmetric Tc−F_c mode. The symmetric counterparts of these modes are strongly coupled, occur at intermediate frequencies, and are assigned to the bands at 553 (Li^+), 587 (Cs^+), and 555 cm^{-1} ($N(CH_3)_4^+$) (symmetric stretch) and at 517 (Li^+), 515 (Cs^+), and 512 cm^{-1} ($N(CH_3)_4^+$) (antisymmetric stretch). The TcO_2 bending mode is assigned to the band at 399, 404 (Li^+), 402 (Cs^+), and 398 cm^{-1} ($N(CH_3)_4^+$) by analogy with the Raman spectra of $ReO_2F_4^-$ and TcO_2F_3, in which it occurs at 402 ($N(CH_3)_4^+$) and 411 cm^{-1}, respectively.

The assignments of the low-frequency bands are anchored by assigning the scissoring modes $\nu_5(A_1)$, $\nu_{11}(B_1)$, and $\nu_{12}(B_1)$ to the most intense of the remaining bands. These assignments were made by comparison with those of OsO_2F_4[7] and $ReO_2F_4^-$ [9,10] and are supported by the theoretical values. Assignments for the remaining modes $\nu_{14}(B_2)$, $\nu_7(A_2)$, $\nu_{15}(B_2)$, $\nu_6(A_1)$, and $\nu_8(A_2)$ are more tentative and are based on the frequencies derived from the LDFT calculations.

The assignments for the $N(CH_3)_4^+$ cation of $N(CH_3)_4^+TcO_2F_4^-$ are based on those for the free cation, which belongs to the point group T_d and has 19 fundamental vibrational bands, $3A_1 + A_2 + 4E + 4T_1 + 7T_2$. Of these, the T_2 modes are infrared active and the A_1, E, and T_2 modes are Raman active. The assignments for the $N(CH_3)_4^+$ cation generally follow those previously given for other $N(CH_3)_4^+$ salts[39−45] and require no further comment. It can be concluded that in $N(CH_3)_4^+TcO_2F_4^-$ the distortion of the $N(CH_3)_4^+$ cation from tetrahedral symmetry is minimal.[43]

The Raman spectrum of the $TcO_2F_3 \cdot CH_3CN$ was recorded in CH_3CN solution at −44 °C. The spectrum is shown in Figure 6, and the frequencies and their assignments are listed in Table 5. Attempts to record the Raman spectrum of solid $TcO_2F_3 \cdot CH_3CN$ at −150 °C resulted in rapid decomposition of the sample to an unidentified dark blue product. The assignments were

(38) In order to evaluate the degree of vibrational coupling within the unit cell of $Li^+TcO_2F_4^-$, a factor-group analysis of the vibrational modes of the $Li^+TcO_2F_4^-$ unit cell was carried out using the correlation method. (Carter, R. J. *J. Chem. Educ.* **1971**, *48*, 297 and references therein.)

(39) Mercier, H. P. A.; Sanders, J. C. P.; Schrobilgen, G. J. *J. Am. Chem. Soc.* **1994**, *116*, 2921.
(40) Berg, R. W. *Spectrochim. Acta, Part A* **1978**, *34A*, 655.
(41) Bottger, G. L.; Geddes, A. L. *Spectrochim. Acta* **1978**, *21*, 1701.
(42) Kabisch, G.; Klose, M. *J. Raman Spectrosc.* **1978**, *7*, 311.
(43) Kabisch, G. *J. Raman Spectrosc.* **1980**, *9*, 279.
(44) Wilson, W. W.; Christe, K. O.; Feng, J.; Bau, R. *Can. J. Chem.* **1989**, *67*, 1898.
(45) Christe, K. O.; Wilson, W. W.; Wilson, R. D.; Bau, R.; Feng, J. *J. Am. Chem. Soc.* **1990**, *112*, 7619.

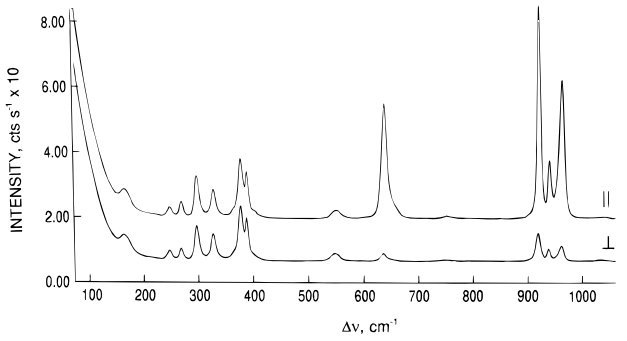

Figure 6. Raman spectrum of a solution of TcO_2F_3 in CH_3CN recorded in a Pyrex tube at −44 °C using 647.1-nm excitation. The upper trace and lower trace are with the analyzer parallel and perpendicular to the polarization of the incident beam, respectively.

made by comparison with calculated frequencies (see Table 5 and Computational Results) and the Raman spectra of CH_3CN,[46] TcO_2F_3,[5] $TcO_2F_4^-$, and the $ReO_2F_3{\cdot}CH_3CN$ adduct in the solid state and in CH_3CN solution.[9] The adduct is expected to have a geometry in which CH_3CN is coordinated to the Tc atom of TcO_2F_3 in a position *trans* to one of the oxygen ligands (see Characterization of $TcO_2F_4^-$ and $TcO_2F_3{\cdot}CH_3CN$ by ^{19}F, ^{99}Tc, and ^{17}O NMR Spectroscopy). On the basis of this assumption, the adduct would possess C_s point symmetry in which case 30 Raman and infrared active vibrational modes are predicted (19A′ + 11A″).

The Raman spectrum of $TcO_2F_3{\cdot}CH_3CN$ in acetonitrile shows three strongly polarized bands in the 900−1000 cm^{-1} region which can readily be assigned to the C−C stretch, $\nu_4(A_1)$, of free CH_3CN (920 cm^{-1}), the TcO_2 antisymmetric stretch (940 cm^{-1}), and the TcO_2 symmetric stretch (963 cm^{-1}). The band corresponding to ν(CC) of complexed CH_3CN is likely coincident with the TcO_2 stretch at 940 cm^{-1} and is consistent with what is observed for $ReO_2F_3{\cdot}CH_3CN$ (943 cm^{-1}). The TcO_2 stretching frequencies of $TcO_2F_3{\cdot}CH_3CN$ are intermediate between those observed for the $[TcO_2F_4]$ unit of TcO_2F_3 and the $TcO_2F_4^-$ anion and are consistent with the formation of a Lewis acid−base adduct. Three bands appear in the Tc−F stretching region including a depolarized band at 549 cm^{-1}, which can only be assigned to the antisymmetric TcF_{2c} stretching mode, while the two polarized modes at 637 and 659 cm^{-1} are assigned to the symmetric TcF_{2c} stretch and the TcF_t stretch, respectively. LDFT calculations show that the symmetric TcF_{2c} stretch is strongly coupled with the TcF_t stretch. The TcO_2 scissor bend is assigned to the strong band at 389 cm^{-1} and is confirmed by the theoretical value calculated at the LDFT level. The remaining low-frequency bands are assigned to strongly coupled bending modes with the aid of frequencies calculated at the LDFT level.

The frequency shifts observed for complexed acetonitrile are comparable to those observed for the $Co(CH_3CN)_6^{2+}$ complex.[47] The ν_8 (378 cm^{-1}), ν_4 (920 cm^{-1}), ν_6 (1448 cm^{-1}), ν_2 (2257 cm^{-1}), and $\nu_3 + \nu_4$ (2297 cm^{-1}) bands of free acetonitrile are shifted to 403, 940, 1416, 2297, and 2325 cm^{-1}, respectively, in $TcO_2F_3{\cdot}CH_3CN$.

Computational Results

Density functional theory has been shown to be a good method for predicting the geometries and vibrational spectra for transition metal compounds.[48] In our previous studies on osmium oxide fluorides,[7] we found that the local level yielded better structural and vibrational predictions than did calculations with gradient (nonlocal) corrections.

Molecular Geometries. The molecular geometries were initially optimized at the local density functional theory (LDFT) level with a polarized double-ζ basis set (DZVP). The structure of monomeric TcO_2F_3 is predicted to have C_{2v} point symmetry (Table 6) with the oxygen atoms and a fluorine atom in the trigonal plane and is in agreement with previous experimental and theoretical findings for the isovalent ReO_2F_3 monomer and the $OsO_2F_3^+$ cation.[8] The D_{3h} structure, with the oxygen atoms in the axial positions, is not a minimum with two imaginary frequencies and is, with a zero point energy correction, 45.3 kcal mol^{-1} higher in energy than the C_{2v} structure. The Tc−O bond distance is predicted to be 1.691 Å in contrast to the experimental Tc−O distances of 1.660 Å in $TcO_2F_4^-$ and 1.646 Å in the TcO_2F_3 extended chain structure.[5] The Tc−F axial and equatorial bonds are predicted to be of the same length, 1.872 Å, which is also longer than the terminal Tc−F bond of 1.834 Å in the TcO_2F_3 extended chain structure. The bond distances calculated using the new polarized triple-ζ valence basis set (TZVP) are shorter by about 0.005 Å compared to the DZVP results. The nonlocal values are longer than the local values following previously observed trends. The O−Tc−O angle is closed down from 120 to 109° as found for $OsO_2F_3^+$ and ReO_2F_3.[8] The F_c−Tc−F_c angle differs from 180° by 18°, and the axial fluorines are bent away from the oxygens, toward the equatorial fluorine as in $OsO_2F_3^+$ and ReO_2F_3.

The energy-minimized structure of the $TcO_2F_3{\cdot}CH_3CN$ adduct corresponds to a *cis*-dioxo arrangement in which the CH_3CN molecule is coordinated *trans* to an oxygen. The calculated geometric parameters of the adduct differ only slightly from those calculated for monomeric TcO_2F_3 (Table 6). The bond distances for the Tc−O bonds differ by almost 0.02 Å with the bond *trans* to the Tc−N bond being shorter. The Tc−F bond *trans* to Tc−O is significantly lengthened by 0.03 Å as compared to the other Tc−F bonds. The bond lengths and angles for the CH_3CN moiety are essentially the same as those of the isolated molecule,[49] and the long Tc−N bond distance, 2.308 Å, is consistent with a donor−acceptor type interaction.[35] Addition of the CH_3CN adduct to trigonal bipyramidal TcO_2F_3 induces significant changes in the angles as the structure more closely approximates an octahedral structure. The O−Tc−O angle decreases by about 5°, and one F_t−Tc−O angle increases by about 30° with the other F_t−Tc−O angle decreasing by a similar amount. The angle between the axial fluorines, ∠F_c−Tc−F_c, decreases by about 4°.

The C_{2v} structure of $TcO_2F_4^-$ (Table 7) has the lowest energy and is 24.1 kcal mol^{-1} more stable than the *trans*-dioxo (D_{4h}) structure, which again has two imaginary frequencies. The calculated Tc−O bond distance of 1.724 Å is 0.064 Å longer than that of $TcO_2F_4^-$ in the crystal. Such an error is somewhat larger than what would be expected based on LDFT calculations on OsO_2F_4,[7] which were done with pseudopotentials. The calculated values for OsO_2F_4 are 0.05 Å longer than the experimental values. The increased error for $TcO_2F_4^-$ could be due to missing relativistic effects which should decrease the bond length by a few hundredths of an angstrom. Another possible source for the differences is that LDFT methods may

(46) (a) Günthard, H. H.; Kováts, E. *Helv. Chim. Acta* **1952**, *35*, 1190. (b) Yamadera, R.; Kremm, S. *Spectrochim. Acta, Part A* **1968**, *24*, 1677.
(47) Reedijk, J.; Zuur, A. P.; Groeneveld, W. L. *Recl. Trav. Chim.* **1967**, *86*, 1127.
(48) Sosa, C.; Andzelm, J.; Elkin, B. C.; Wimmer, E.; Dobbs, K. D.; Dixon, D. A. *J. Phys. Chem.* **1992**, *96*, 6630.
(49) Karakida, K.; Fukuyama, T.; Kuchitsu, K. *Bull. Chem. Soc. Jpn.* **1974**, *47*, 299.

Table 5. Experimental Raman and Calculated Vibrational Frequencies, Assignments, and Mode Descriptions for $TcO_2F_3 \cdot CH_3CN$

frequencies (cm^{-1})		
expt[a]	LDFT/DZVP[b]	assgnts in C_s pt sym[c]
3010 (5), dp[d,e]	3092 (3)	$\nu_{20}(A'')$, $\nu_{as}(CH_3)$
3010 (5), dp[d,e]	3087 (3)	$\nu_{21}(A'')$, $\nu_{as}(CH_3)$
2950 (75), p[d]	2990 (2)	$\nu_1(A')$, $\nu_{sym}(CH_3)$
2325 (8), p		$\nu_3 + \nu_7(A')$
2297 (11), p[d]	2373 (92)	$\nu_2(A')$, $\nu(CN)$
1416 (5), dp[e]	1404 (18)	$\nu_{22}(A'')$, $\delta_{as}(CH_3)$
1416 (5), dp[e]	1396 (17)	$\nu_{23}(A'')$, $\delta_{as}(CH_3)$
1375 (15), p[d]	1347 (11)	$\nu_3(A')$, $\delta_{sym}(CH_3)$
1039 (1), dp	990 (8)	$\nu_4(A')$, $\delta_{rock}(CH_3) + \delta(NCC)$
1020 (1), dp	985 (19)	$\nu_5(A')$, $\delta_{rock}(CH_3) + \nu(TcO_t) + \delta(NCC)$
963 (65), p	984 (127)	$\nu_6(A')$, $\nu(TcO_t) + \delta_{rock}(CH_3) + \delta(NCC)$
940 (28), p[e]	982 (41)	$\nu_7(A')$, $\nu(TcN) - \nu(CC)$
940 (28), p[e]	943 (123)	$\nu_8(A')$, $\nu(TcO_c)$
807 (1), dp		$2\nu_{11}$ (A')
659 (6), sh, p	658 (57)	$\nu_9(A')$, $\nu_{sym}(TcF_{2c}) + \nu(TcF_t)$
637 (53), p	584 (27)	$\nu_{10}(A')$, $\nu_{sym}(TcF_{2c}) - \nu(TcF_t)$
549 (6), dp	685 (198)	$\nu_{24}(A'')$, $\nu_{as}(TcF_{2c})$
413 (3), sh		
403 (6), sh	405 (0.5)	$\nu_{11}(A')$, $\delta(TcNC) + \delta(NCC)$
389 (35), dp	366 (6)	$\nu_{12}(A')$, $\delta(TcO_2)$
363 (7), sh, dp	376 (0.6)	$\nu_{13}(A')$, $\delta(TcNC) + \delta(NCC)$
328 (20), dp	325 (1)	$\nu_{25}(A'')$, $\delta(O_tTcF_c) + \delta(F_cTcF_t)$
	291 (22)	$\nu_{14}(A')$, $\delta(O_tTcF_t) - \delta(O_cTcF_t) + \delta(F_cTcF_c)$
298 (28), dp	288 (16)	$\nu_{26}(A'')$, oop $\delta(O_cTcF_t) - \delta(O_cTcF_t) + \delta(O_tTcF_t)$
270 (10), p	260 (12)	$\nu_{15}(A')$, $\delta(F_tTcN) + \delta(F_cTcF_c) - \delta(NCC)$
248 (6), dp	228 (12)	$\nu_{27}(A'')$, oop $\delta(NTcF_c) - \delta(NTcF_c) + (O_tTcF_t)$ wag
217 (2), dp	208 (10)	$\nu_{16}(A')$, $\nu(TcN)$
	203 (2)	$\nu_{17}(A')$, $\delta(F_cTcF_c) - \delta(NTcO_c)$
165 (20), dp	160 (0.3)	$\nu_{18}(A')$, $\delta(F_cTcF_c) - \delta(O_tTcF_t)$
	146 (1)	$\nu_{28}(A'')$, oop $\delta(O_cTcN) - (O_tTcF_t)$ wag
	65 (4)	$\nu_{19}(A')$, ip $\delta(CNTc)$
	44 (4)	$\nu_{29}(A'')$, oop $\delta(CNTc)$
	64i[f]	$\nu_{30}(A')$, CH_3 torsion

[a] Solution spectrum recorded in a Pyrex glass tube at −44 °C using 647.1-nm excitation. Values in parentheses denote relative Raman intensities; sh = shoulder, p = polarized band, and dp = depolarized band. Frequencies observed for free CH_3CN (C_{3v} point symmetry): $\nu_5(E)$, 3010 (5), $\nu_1(A_1)$, 2950 (75), $2\nu_6$, 2886 (2), $2\nu_7 + 2\nu_8$, 2848 (1), $2\nu_3$, 2738 (2), $\nu_3 + \nu_4(A_1)$, 2297 (11), $\nu_2(A_1)$, 2257 (78), $2\nu_4 + \nu_8$, 2208 (1), $\nu_6(E)$, 1448 (6), $\nu_3(A_1)$, 1375 (15), $\nu_7(E)$, 1039 (1), $\nu_4(A_1)$ 920 (100), $2\nu_8$, 807 (1), $\nu_8(E)$, 379 (5). [b] Infrared intensities, in km mol^{-1}, are given in parentheses. [c] The atom labeling scheme is given by structure **II**; oop and ip denote out-of-plane and in-plane, respectively. [d] Coincident with a mode of free CH_3CN. [e] Coincident modes. [f] A number of different rotomers involving the CH_3 were investigated. All gave a low imaginary frequency for the torsion. This is typical of DFT grid-based calculations.

Table 6. Geometric Parameters for Monomeric TcO_2F_3 and $TcO_2F_3 \cdot CH_3CN$

	TcO_2F_3[a]					$TcO_2F_3 \cdot CH_3CN$[b]
	LDFT		NLDFT			LDFT
bond length/angle	TZVP	DZVP	TZVP	DZVP	expt[c]	DZVP
Tc−O (Å)	1.686	1.691	1.704	1.709	1.646(9)	1.711 [1.692]
Tc−F_t (Å)	1.866	1.872	1.895	1.902		1.910
Tc−F_c (Å) (term)	1.862	1.872	1.893	1.900	1.834(7)	1.879, 1.881
O−Tc−O (deg)	109.0	108.5	109.1	108.7		103.9
F_t−Tc−O (deg)	125.5	125.7	125.5	125.7		157.3 [98.8]
F_c−Tc−F_c (deg)	162.0	161.8	162.0	162.1		158.0
F_c−Tc−F_t (deg)	81.0	80.9	81.0	81.1		83.0, 83.0
O−Tc−F_c (deg)	95.2	95.3	95.2	95.2		93.2, 93.2 [99.5, 99.3]

[a] For simplicity, the F_{eq} and F_{ax} of the trigonal bipyramidal TcO_2F_3 monomer are also described as F_t and F_c, respectively. [b] Values involving Tc−O *trans* to F_t are reported without brackets and values involving Tc−O *trans* to the N are reported in brackets. Other calculated values for the CH_3CN group: Tc−N, 2.308 Å; C−N, 1.162 Å; C−C, 1.439 Å; C−H, 1.104 Å; O−Tc−N, 81.6° [174.4]°; F_c−Tc−N, 80.7, 79.5°; F_t−Tc−N, 75.7°; Tc−N−C, 175.8°; N−C−C, 178.9°; C−C−H, 110.1°. [c] Experimental values are taken from polymeric TcO_2F_3.[5]

not perform as well for anions as for neutral molecules or cations. The Tc−F_t bond length for the fluorines *trans* to oxygen is 1.946 Å and is longer than the Tc−F_c bond length of 1.910 Å. Both bond distances are longer than those of monomeric TcO_2F_3, as expected for a structure in which a fluoride ion has been added. Comparison to experiment shows that the calculated Tc−F_c bond length is 0.034 Å longer whereas the predicted Tc−F_t bond length is 0.040 Å shorter than the experimental distances. Calculations with the TZVP basis set gave similar results with bond distances shorter by about 0.01 Å than those obtained with the DZVP basis set. This suggests that there is a strong interaction between the Li^+ and the *trans*-fluorines in the crystal (see X-ray Crystal Structure of $Li^+TcO_2F_4^-$). The calculated angles for $TcO_2F_4^-$ are in good agreement with the experimental values for the extended chain structure. The largest differences are for the F_c−Tc−F_c angle, which is calculated to be 4° larger than the experimental value, and for the F_t−Tc−F_t angle, which is predicted to be about 3°

Table 7. Geometric Parameters for $TcO_2F_4^-$ (C_{2v})

	LDFT		NLDFT		
bond length/angle	TZVP	DZVP	TZVP	DZVP	expt
Tc−O (Å)	1.715	1.724	1.734	1.724	1.660(4)
Tc−F_t (Å)	1.938	1.946	1.975	1.946	1.986(3)
Tc−F_c (Å)	1.899	1.910	1.935	1.910	1.876(3)
O−Tc−O (deg)	101.3	101.6	101.3	101.3	102.5(3)
F_t−Tc−O (deg)	89.7	89.6	89.6	89.6	90.4(2)
F_c−Tc−F_c (deg)	168.3	168.0	168.6	168.6	164.2(3)
F_c−Tc−F_t (deg)	85.5	85.4	85.6	85.6	83.8(1)
O−Tc−F_c (deg)	93.7	93.8	93.6	93.6	94.9(1)
F_t−Tc−F_t (deg)	79.5	79.5	79.2	79.3	76.7(2)

larger than the experimental value. These angles involve the most ionic bonds and would be expected to exhibit the largest distortions arising from the long contacts to the Li^+ cation (see X-ray Crystal Structure of $Li^+TcO_2F_4^-$).

Charges, Valencies, Bond Orders, and Valence Orbital Populations. Calculated charges and valencies are given in Table 8. The DZVP charges show the technetium of the TcO_2F_3 monomer to have a charge of about +1.3 and negative charges of about −0.2 on the oxygens and −0.3 on the fluorine atoms. The larger TZVP basis set gives a higher ionic character with a charge of about +1.8 on the technetium atom and charges of −0.3 and −0.4 on the oxygen and fluorine atoms, respectively. The Mayer valencies[50] show a valency of 6.27 for technetium with valencies of 2.50 for oxygen and 1.14 and 1.16 for the two fluorine atoms (Table 9). The Mayer bond order is 1.87 for the Tc−O bond showing that this bond is essentially a double bond whereas the Tc−F bond orders are 0.84, which are slightly less than for a single bond. For $TcO_2F_4^-$, the addition of a fluoride ion slightly decreases the charge on technetium at the DZVP level and increases it slightly at the TZVP level. Most of the additional negative charge is equally distributed among the oxygen and fluorine atoms. At the DZVP level, the Mayer valency at technetium increases by 0.39 over that in TcO_2F_3 to 6.66. The empirical bond valency of 6.78 derived using the method of Brown[32] (Table 3) is in good agreement with the more rigorously derived and calculated Mayer value. The oxygen and fluorine valencies decrease somewhat in the anion, but the changes are small. The Mayer bond orders also show only small changes in going to the anion. The Tc−O bond order is 1.81, and the Tc−F_t and Tc−F_c bond orders decrease to 0.74 and 0.77, respectively. Increasing the size of the basis set or adding nonlocal corrections lowers both Mayer valencies and bond orders, but the conclusions remain the same. The charges for the $TcO_2F_3{\cdot}CH_3CN$ adduct show slight changes from that of TcO_2F_3 with the technetium having slightly less positive charge. The valency at technetium increases from 6.27 in TcO_2F_3 to only 6.42 in the adduct showing a weak interaction with the nitrogen atom and is consistent with the Mayer bond order of 0.22 for the Tc−N bond.

The valence orbital populations on the Tc atoms show that the electrons are predominantly in the d orbitals. For TcO_2F_3, there are 5.15 electrons in the valence d orbitals and 0.48 electrons in the valence p orbitals at the DZVP/LDFT level. With the TZVP basis set, there is no p population and the 5.25 valence electrons are divided between the d orbitals (5.12 e) and the f orbitals (0.13 e). For the anion, $TcO_2F_4^-$, there is little change in the populations with the increased electron density being essentially distributed among the valence p orbitals (0.56 e) and d orbitals (5.21 e) at the DZVP level. The valence d orbital charge distributions average 1.02−1.03 in the d_{xy}, d_{xz}, and d_{yz} and 0.73−0.74 in the $d_{x^2-y^2}$ and d_{z^2} orbitals for the three compounds studied and are in accord with the strong π-donor properties of the oxygen atoms to the approximately $d_{t_{2g}}$ technetium orbitals.

Vibrational Frequencies. The calculated vibrational frequencies for the TcO_2F_3 monomer are compared to the previously reported experimental Raman values[5] for the solid-state chain structure in Table 10. The calculated TcO_2 symmetric stretching frequency is slightly higher than the antisymmetric component paralleling the experimental findings. Very little scaling would be needed between the DZVP or TZVP values and the experimental values at the LDFT level. The Tc−F stretches and bends are in reasonable agreement with the experimental values for the two methods, with the largest differences occurring for deformation modes involving the TcO_2 moiety. Surprisingly, as the calculated values are harmonic, the TcO_2 symmetric bend $\nu_4(A_1)$ is too low by 76 cm^{-1} and the $\nu_5(A_1)$ mode involving TcO_2 and TcF_{2c}/TcF_{2t} scissoring is too low by about 50 cm^{-1}. Difficulty in predicting the MO_2 bend was also encountered for OsO_2F_4[7] and arises because repulsion between the oxygen atoms is not adequately accounted for in the calculations. The decrease in the O−Tc−O bending frequency is consistent with the long Tc−O bond lengths in terms of this repulsion argument. The nonlocal level frequencies are lower as would be expected from the increased bond lengths. There is very little difference in the vibrational spectra for the two basis sets at the local level or at the nonlocal level.

For $TcO_2F_4^-$, the calculated and experimental frequencies exhibit somewhat different behavior. The calculated stretches at the local level are lower than the experimental values but only by a few cm^{-1}. As would be expected, the TcO_2 scissor is too low although the difference is smaller for the anion than for TcO_2F_3, but the other bending frequencies are in good agreement with the experimental values.

The calculated vibrational frequencies of the $TcO_2F_3{\cdot}CH_3CN$ adduct also show good agreement with the experimental frequencies. The CN triple bond stretch is predicted to be at 2373 cm^{-1} compared to the experimental value of 2297 cm^{-1}. The Tc−O stretching modes now split with the Tc−O *trans* to the nitrogen atom having a higher frequency than the Tc−O *cis* to the nitrogen atom. The C−C stretch couples with the CH_3 rocks and also slightly with the Tc−N stretch. However, the Tc−N stretch occurs at a much lower value of 208 cm^{-1}. The remainder of the spectrum is in good agreement with the experiment, and again the TcO_2 bend is predicted to be lower than the experimental value.

NMR Chemical Shifts. It is now possible to calculate NMR chemical shifts by *ab initio* theoretical methods. Three different approaches, all within the DFT formalism, have been used in the present work for treatment of the gauge invariance problem: the IGLO[51] and LORG[52] treatments in an uncoupled DFT approach[53] and the GIAO approach.[54] The standards used for

(50) Mayer, I. *Chem. Phys. Lett.* **1983**, *97*, 270. Mayer, I. *Theoret. Chim. Acta* **1985**, *67*, 315. Mayer, I. *J. Quantum Chem.* **1986**, *29*, 73. Mayer, I. *J. Quantum Chem.* **1986**, *29*, 477.

(51) Kutzelnigg, W. *Isr. J. Chem.* **1980**, *19*, 193. Schindler, M.; Kutzelnigg, W. *J. Chem. Phys.* **1982**, *76*, 1919.

(52) Hansen, A. E.; Bouman, T. D. *J. Chem. Phys.* **1985**, *82*, 5035.

(53) Arduengo, A. J., III; Dixon, D. A.; Kumashiro, K. K.; Lee, C.; Power, W. P.; Zilm, K. W. *J. Am. Chem. Soc.* **1994**, *116*, 6361.

(54) Cheeseman, J. R.; Trucks, G. W.; Keith, T. A.; Frisch, M. J. *J. Chem. Phys.* **1996**, *104*, 5497. London, F. J. *Phys. Radium (Paris)* **1937**, *8*, 397. Ditchfield, R. *Mol. Phys.* **1974**, *27*, 789. Wolinski, K.; Hinton, J. F.; Pulay, P. *J. Am. Chem. Soc.* **1990**, *112*, 8251.

(55) (a) Beattie, I. R.; Crocombe, R. A.; Ogden, J. S. *J. Chem. Soc., Dalton Trans.* **1977**, 1481. (b) Brisdon, A. K.; Holloway, J. H.; Hope, E. G.; Townson, P. J.; Levason, W.; Ogden, J. S. *J. Chem. Soc., Dalton Trans.* **1991**, 3127.

Table 8. Atomic Charges (e) for Monomeric TcO_2F_3, $TcO_2F_3 \cdot CH_3CN$, and $TcO_2F_4^-$

	TcO_2F_3[a]				$TcO_2F_3 \cdot CH_3CN$[b]	$TcO_2F_4^-$			
	LDFT		NLDFT		LDFT	LDFT		NLDFT	
atom	TZVP	DZVP	TZVP	DZVP	DZVP	TZVP	DZVP	TZVP	DZVP
Tc	1.77	1.27	1.80	1.36	1.18	1.83	1.08	1.91	1.22
O	−0.30	−0.21	−0.30	−0.23	−0.22 [−0.21]	−0.41	−0.30	−0.43	−0.53
F_t	−0.41	−0.29	−0.41	−0.31	−0.32	−0.52	−0.38	−0.53	−0.41
F_c	−0.38	−0.28	−0.40	−0.30	−0.30, −0.30	−0.48	−0.36	−0.49	−0.38

[a] For simplicity, the F_{eq} and F_{ax} of the trigonal bipyramidal TcO_2F_3 monomer are also described as F_t and F_c, respectively. [b] Values involving Tc−O *trans* to F_t are reported without brackets and values involving Tc−O *trans* to the N are reported in brackets. Other calculated values for the CH_3CN group: N, −0.06; C, 0.06; $C(H_3)$, −0.71; H, 0.29.

Table 9. Mayer Valencies and Mayer Bond Orders for TcO_2F_3, $TcO_2F_3 \cdot CH_3CN$, and $TcO_2F_4^-$

	Mayer valencies											
	TcO_2F_3[a]				$TcO_2F_3 \cdot CH_3CN$[b]				$TcO_2F_4^-$			
	Tc	O	F_t	F_c	Tc	O	F_t	F_c	Tc	O	F_t	T_c
LDFT/DZVP	6.27	2.50	1.16	1.14	6.42	2.48 [2.51]	1.10	1.15, 1.15	6.66	2.43	1.01	1.05
LDFT/TZVP	5.95	2.46	1.04	1.04					6.08	2.40	0.83	0.91
NLDFT/DZVP	6.13	2.48	1.14	1.16					6.45	2.40	0.98	1.01
NLDFT/TZVP	5.91	2.44	1.01	1.03					5.98	2.36	0.82	0.88

	Mayer bond orders								
	TcO_2F_3[a]			$TcO_2F_3 \cdot CH_3CN$[b]			$TcO_2F_4^-$		
	Tc−O	Tc−F_t	Tc−F_c	Tc−O	Tc−F_t	Tc−F_c	Tc−O	Tc−F_t	Tc−T_c
LDFT/DZVP	1.87	0.84	0.84	1.86 [1.87]	0.79	0.83, 0.84	1.81	0.74	0.77
LDFT/TZVP	1.86	0.76	0.73				1.79	0.60	0.65
NLDFT/DZVP	1.84	0.81	0.81				1.79	0.71	0.73
NLDFT/TZVP	1.86	0.74	0.72				1.77	0.59	0.63

[a] For simplicity, the F_{eq} and F_{ax} of the trigonal bipyramidal TcO_2F_3 monomer are also described as F_t and F_c, respectively. [b] Values involving Tc−O *trans* to F_t are reported without brackets and values involving Tc−O *trans* to the N are reported in brackets. Other calculated values for the CH_3CN group are as follows. Mayer valencies: N, 3.37; C, 3.99; $C(H_3)$, 3.76; H, 0.88. Mayer bond orders: Tc−N, 0.22; C−N, 2.95; C−C, 1.03; C−H, 0.88.

Table 10. Experimental Raman Frequencies for TcO_2F_3 in the Solid State and Calculated Vibrational Frequencies, Assignments, and Mode Descriptions for Monomeric TcO_2F_3

	frequencies (cm^{-1})				
	LDFT[b]		NLDFT[b]		
expt[a]	TZVP	DZVP	TZVP	DZVP	assgnts for TcO_2F_3 in C_{2v} pt sym
974 (100)	1009 (58)	990 (68)	966 (55)	952 (64)	$\nu_1(A_1)$, $\nu_{sym}(TcO_2)$
963 (27), 958 sh	1003 (107)	983 (118)	959 (99)	943 (110)	$\nu_7(B_1)$, $\nu_{as}(TcO_2)$
685(3), 670 (7)	700 (196)	703 (203)	660 (186)	667 (191)	$\nu_{10}(B_2)$, $\nu_{as}(TcF_{2c})$
650(16), 632 (16)	695 (69)	698 (68)	658 (66)	659 (64)	$\nu_2(A_1)$, $\nu_{sym}(TcF_{2c} + TcF_t)$
	606 (10)	607 (10)	571 (8)	574 (9)	$\nu_3(A_1)$, $\nu_{sym}(TcF_{2c} - TcF_t)$
416 sh, 411 (19)	340 (2)	343 (1)	334 (2)	336 (1)	$\nu_4(A_1)$, $\delta_{sciss}(TcO_2)$
320 (22)	355 (0)	351 (0)	347 (0)	340 (0)	$\nu_{11}(B_2)$, $\delta_{sciss}(TcF_cF_t)$
295 (30)	247 (7)	243 (9)	243 (7)	237 (9)	$\nu_5(A_1)$, antisym comb of TcO_2 sciss and TcF_{2c} sciss
284 (24)	295 (0)	298 (0)	288 (0)	293 (0)	$\nu_6(A_2)$, TcO_2 torsion
278 sh	264 (9)	272 (8)	256 (9)	266 (8)	$\nu_8(B_1)$, antisym comb of $TcOF_t$ sciss and TcF_cF_t sciss
264 (2)	263 (36)	260 (0)	263 (34)	260 (32)	$\nu_{12}(B_2)$, $\delta_{umbrella}(TcO_2F_t)$
	31 (0)	66 (0)	19 (0)	67 (0)	$\nu_9(B_1)$, sym comb of $TcOF_t$ sciss and TcF_cF_t sciss

[a] Values in parentheses denote relative Raman intensities, and sh = shoulder. [b] Infrared intensities, in km mol^{-1}, are given in parentheses.

the relative chemical shift calculations are TcO_4^- for ^{99}Tc, $CFCl_3$ for ^{19}F, and H_2O for ^{17}O.

The relative chemical shift of ^{99}Tc in TcO_2F_3 is calculated to be 340 and 348 ppm at the DZVP/IGLO and DZVP/LORG levels, respectively. With the larger TZ2P basis set, the relative shift is predicted to be 275 ppm at the GIAO level. All three methods show that addition of a fluoride ion to TcO_2F_3 results in significant deshielding of ^{99}Tc to *ca.* 600 ppm. The values predicted for $TcO_2F_4^-$, however, are not in good agreement with the experimental value of 343 ppm. Surprisingly, the formation of the $TcO_2F_3 \cdot CH_3CN$ adduct only results in a small shielding of the chemical shift (78 ppm) compared to that of $TcO_2F_4^-$ as measured experimentally, whereas the theoretical chemical shift of $TcO_2F_3 \cdot CH_3CN$ is *ca.* 430 ppm more shielded than that of $TcO_2F_4^-$ and *ca.* 170 ppm more shielded than that of TcO_2F_3. The large discrepancy between experiment and theory could be due to the fact that the shifts were calculated for the isolated free gas-phase ion or neutral as compared to the experimental measurements which were carried out in solution. Additional reasons for the discrepancies are potential deficiencies in the Tc basis set and the potential importance of relativistic effects.

The calculated ^{17}O chemical shift for $TcO_2F_4^-$ is 30 ppm less than the experimental value of 1204 ppm, and the chemical shift of free TcO_2F_3 is deshielded relative to that of the anion by 50−60 ppm at the IGLO/DZVP or LORG/DZVP levels and by 13 ppm at the GIAO/TZ2P level. Formation of the adduct

$TcO_2F_3 \cdot CH_3CN$ not only splits the two oxygen atom peaks by about 25 ppm but also deshields them relative to the oxygen atoms in TcO_2F_3 and $TcO_2F_4^-$. This contrasts with the experimental observation of no chemical shift difference between the oxygens in the adduct and in $TcO_2F_4^-$, which is attributed to exchange averaging (see Characterization of $TcO_2F_4^-$ and $TcO_2F_3 \cdot CH_3CN$ by ^{19}F, ^{99}Tc, an ^{17}O NMR Spectroscopy).

The ^{19}F shifts show the most difference between theory and experiment. The experimental fluorine chemical shifts differ only slightly from that of the standard, $CFCl_3$, and only small chemical shift differences are predicted for the equatorial (*cis*)/axial (*trans*) pairs. The computational results are quite different. For example, the fluorine chemical shifts of TcO_2F_3 are predicted to be significantly more deshielded relative to $CFCl_3$ and the splitting of the two peaks is predicted to be 228, 225, and 117 ppm at the IGLO/DZVP, LORG/DZVP, and GIAO/TZ2P levels. The equatorial (*trans*) shifts are always predicted to be deshielded with respect to the chemical shift of the axial (*cis*) shifts. The chemical shifts for $TcO_2F_4^-$ are predicted to be shielded with respect to those of TcO_2F_3, and the chemical shift difference between the two fluorine environments decreases to 114, 104, and 76 ppm at the IGLO/DZVP, LORG/DZVP, and GIAO/TZ2p levels, respectively. The absolute chemical shifts for the $TcO_2F_3 \cdot CH_3CN$ adduct are predicted to occur between those of TcO_2F_3 and $TcO_2F_4^-$, but the axial/equatorial chemical shift difference is predicted to be much smaller, 51 ppm at the IGLO/DZVP level and 81 ppm at the LORG/DZVP level. Improving the basis set and going to the GIAO level would lead to a further decrease in the chemical shift difference on the basis of the calculations for TcO_2F_3 and $TcO_2F_4^-$.

Conclusion

Technetium dioxide trifluoride behaves as an electron pair acceptor toward fluoride ion and CH_3CN forming $TcO_2F_4^-$ and $TcO_2F_3 \cdot CH_3CN$ which both occur as *cis*-dioxo isomers. The energy-minimized geometries determined from density functional theory calculations are in agreement with the structures determined by X-ray crystallography and by NMR and Raman spectroscopy. The energy-minimized geometry of TcO_2F_3 monomer is a trigonal bipyramid with the oxygens *cis* and in the equatorial plane as observed experimentally for the matrix-isolated ReO_2F_3[55] and the $OsO_2F_3^+$ cation in SbF_5 solution.[8]

Experimental Section

All operations were conducted in laboratories that were monitored routinely by the McMaster University Health Physics Group for radioactive contamination. All work involving ^{99}Tc was licensed and performed according to the regulations and recommendations of the Canadian Atomic Energy Control Board.[56]

Apparatus and Materials. Volatile materials were handled in vacuum lines constructed of nickel, stainless steel, FEP, and Pyrex vacuum lines, as previously described.[57] Nonvolatile materials were handled in the dry nitrogen atmosphere of a glovebox.

Anhydrous $N(CH_3)_4F$ was prepared according to the literature method of Christe *et al.*[45] Lithium fluoride (Research Inorganic Chemicals) and cesium fluoride (Merck) were dried as described previously.[58] The solvents, CH_3CN (HPLC Grade, Caledon Laboratories Ltd.)[59] and HF (Harshaw Chemical Co.),[60] were dried/purified by the standard literature methods.

Preparation and Decomposition of $TcO_2F_3 \cdot CH_3CN$. In the drybox, 0.0202 g (0.108 mmol) of TcO_2F_3 was loaded into a 4-mm-o.d. FEP tube fitted with a Kel-F valve. Approximately 0.3 mL of dry CH_3CN was condensed onto the TcO_2F_3 which completely dissolved to give a clear yellow solution. The reactor was then heat-sealed and stored in liquid nitrogen until the NMR experiment was performed. Another sample was prepared by dissolving 0.0316 g (0.168 mmol) of TcO_2F_3 in 0.0439 g (1.069 mmol) of dry CH_3CN in a 4-mm-o.d. FEP tube followed by addition of *ca.* 0.2 mL of SO_2ClF.

In the drybox, 0.0423 g (0.225 mmol) of TcO_2F_3 was loaded into a $^1/_4$-in o.d. FEP tube fitted with a Kel-F valve. Approximately 2 mL of dry CH_3CN was condensed onto the solid, which dissolved to form a yellow solution. The solvent was then pumped out at −40 °C over a period of 3 h to yield a light orange solid. The reactor was back-filled with dry nitrogen and warmed to room temperature. Over the next 3 h, the solid turned yellow again and was shown to be TcO_2F_3 by Raman spectroscopy.

Synthesis of $N(CH_3)_4^+TcO_2F_4^-$. In a typical preparation, 0.0652 g (0.347 mmol) of TcO_2F_3 and 0.0328 g (0.352 mmol) of $N(CH_3)_4F$ were loaded inside the dry box into a $^1/_4$-in-o.d. FEP tube fitted with a Kel-F valve. Approximately 3 mL of anhydrous HF was condensed onto the solids, which did not dissolve entirely upon warming the orange solution to room temperature, even after 30 min of vigorous agitation. The solvent was then pumped off, and the microcrystalline orange solid was dried under vacuum for 6 h, pressurized with dry N_2, and stored in the drybox.

A sample for ^{19}F and ^{99}Tc NMR spectroscopy was prepared by weighing 0.0320 g (0.170 mmol) of TcO_2F_3 and 0.0162 g (0.174 mmol) of $N(CH_3)_4F$ into a 4-mm-o.d. FEP NMR tube inside the drybox and condensing anhydrous HF (*ca.* 0.2 mL) onto the solids. After 30 min of vigorous agitation at room temperature, the solvent was pumped off and the light orange solid was dried under dynamic vacuum overnight. Dry CH_3CN was then condensed into the NMR tube, which was then heat-sealed. Before the NMR spectrum was run, the undissolved pale orange solid was centrifuged to the top of the FEP sample tube.

Syntheses of $M^+TcO_2F_4^-$ (M = Li, Cs) and Crystal Growth of $Li^+TcO_2F_4^-$. In a typical preparation, 0.0591 g (0.315 mmol) of TcO_2F_3 and 0.00990 g (0.382 mmol) of finely powdered LiF were loaded inside the drybox into a $^1/_4$-in-o.d. FEP tube fitted with a Kel-F valve. Approximately 1 mL of anhydrous HF was condensed onto the solid, which did not dissolve entirely upon warming the solution to room temperature. The orange solution was agitated vigorously for 30 min before pumping off the solvent at room temperature. The microcrystalline orange $Li^+TcO_2F_4^-$ was then dried under vacuum for 6 h and stored in the drybox. The cesium salt of $TcO_2F_4^-$ was similarly prepared by allowing 0.0618 g (0.329 mmol) of TcO_2F_3 to react with 0.0512 g (0.337 mmol) of CsF.

Single crystals of $Li^+TcO_2F_4^-$ suitable for X-ray structure determination were prepared by the following method: lithium fluoride (0.0062 g, 0.24 mmol) and TcO_2F_3 (0.0304 g, 0.162 mmol) were weighed inside the drybox into one arm of a T-shaped FEP reactor constructed from $^1/_4$-in-o.d. FEP tubes and fitted with a Kel-F valve and anhydrous HF (*ca.* 1 mL) was condensed onto the solids. Excess LiF was necessary to completely solubilize the TcO_2F_3. The reactor was then pressurized to 900 Torr with dry nitrogen and clamped in a horizontal position with the empty side arm immersed in a water/ice bath. The HF slowly condensed into the cooler part of the reactor over a period of 3 days, concentrating the solution until small deep-orange plates formed. The solution was then decanted off the crystals, the reactor was connected to a vacuum line, and the residual HF was pumped off under dynamic vacuum for 12 h.

The reactor was then transferred to a drybox equipped with a microscope, and the crystals were removed by cutting open the FEP tube and prying them off the walls with a steel needle. The crystals

(56) AECB Radioisotope Safety Poster INFO-0142-1/Rev. 2, Rules for Working with Radioisotopes in a Basic Laboratory.
(57) Syvret, R. G.; Schrobilgen, G. J. *Inorg. Chem.* **1989**, *28*, 1564.
(58) Christe, K. O.; Curtis, E. C.; Dixon, D. A.; Mercier, H. P. A.; Sanders, J. C. P.; Schrobilgen, G. J. *J. Am. Chem. Soc.* **1991**, *113*, 3351.
(59) Winfield, J. M. *J. Fluorine Chem.* **1984**, *25*, 91.
(60) Emara, A. A. A.; Schrobilgen, G. J. *Inorg. Chem.* **1992**, *31*, 1323.

were then sealed in Lindemann and quartz capillaries (0.3- and 0.5-mm-i.d., respectively). The crystal used for the data acquisition had the dimensions 0.58 × 0.56 × 0.15 mm.

Crystal Structure Determination. The crystal was centered on a Syntex $P2_1$ diffractometer, using silver radiation monochromatized with a graphite crystal ($\lambda = 0.560\,86$ Å). Accurate cell dimensions were determined at 22 °C from a least-squares refinement of the setting angles (χ, ϕ, and 2θ) obtained from 27 accurately centered reflections (with $15° \leq 2\theta \leq 25°$) chosen from a variety of points in reciprocal space. Integrated diffraction intensities were collected by a $\theta-2\theta$ scan technique with scan rates varying from 1.5 to 14.65°/min (in 2θ) and a scan range of ±0.5° so that the weaker reflections were examined more slowly to minimize counting errors. The data were collected with $-7 \leq h \leq 8$, $0 \leq k \leq 8$, and $0 \leq l \leq 15$ and $3 \leq 2\theta \leq 60°$. During data collection, the intensities of three standard reflections were monitored every 97 reflections to check for crystal stability and alignment; no decay was observed during data collection. In total, 1132 reflections were collected. A total of 523 unique reflections remained after averaging of equivalent reflections. An empirical absorption correction was applied to the data with a ψ-scan method ($\Delta\phi = 10°$) ($\mu\bar{R} = 0.215$). Corrections were made for Lorentz and polarization effects.

Solution and Refinement of the Structure. The XPREP program[61] was used to confirm the unit cell dimensions the crystal lattice. A solution was obtained by using a Patterson function which located the special position of the Tc atom (mm). Successive difference Fourier syntheses revealed the special position of the remaining oxygen, fluorine, and lithium atoms. The final refinement was obtained by introducing anisotropic parameters for all the atoms and a weight factor ($w = 1/\sigma^2(F) + 0.0006F^2$) and gave rise to a residual, R, of 0.0339 ($R_w = 0.0320$). In the final difference Fourier map, the maximum and the minimum electron densities were +1.89 and −1.82 e Å^{-3}.

All calculations were performed on a 486 personal computer using the SHELXTL PLUS determination package[61] for structure solution and refinement as well as structure determination molecular graphics.

Nuclear Magnetic Resonance Spectroscopy. Nuclear magnetic resonance spectra were recorded unlocked (field drift < 0.1 Hz h^{-1}) on Bruker AM-500 (11.744 T) and AC-300 (7.0463 T) spectrometers equipped with Aspect 3000 computers. The ^{19}F spectra were acquired with a 5-mm combination ^{1}H/^{19}F probe. The ^{99}Tc and ^{17}O spectra were obtained with a 10-mm broad-band VSP probe (tunable over the range 23−202 MHz). The ^{1}H and ^{13}C spectra were obtained using a 5-mm ^{1}H/^{13}C/^{19}F/^{31}P combination probe. The ^{19}F (470.599 MHz) spectra were recorded at 11.744 T using a ∼90° pulse width of 1 μs. A total of 2000 and 4000 transients were acquired in 16K memories using spectral width settings of 12 and 25 kHz, acquisition times of 0.688 and 0.328 s, and resolutions of 1.45 and 3.05 Hz/data point for $N(CH_3)_4^+TcO_2F_4^-$ and $TcO_2F_3{\cdot}CH_3CN$, respectively. The free induction decays were multiplied by a Gaussian function using line broadenings of 1 and 3 Hz and a Gaussian broadening factor of 0.27 and 0.20 prior to Fourier transformation. The ^{99}Tc (112.542 MHz) spectra were recorded at 11.744 T using a ∼90° pulse width of 14 μs. A total of 2000 and 1000 transients were acquired in 16K memories using spectral width settings of 25 and 50 kHz, acquisition times of 0.328 and 0.164 s, and resolutions of 3.05 and 6.10 Hz/data point for $N(CH_3)_4^+TcO_2F_4^-$ and $TcO_2F_3{\cdot}CH_3CN$, respectively. The free induction decays were multiplied by a Gaussian function using a line broadening of −150 Hz and a Gaussian broadening factor of 0.015 prior to Fourier transformation for the $N(CH_3)_4^+TcO_2F_4^-$ sample. A line broadening of 10 Hz was used for the $TcO_2F_3{\cdot}CH_3CN$ sample. The ^{17}O (67.801 MHz) spectra were recorded at 11.744 T using a ∼90° pulse width of 6.4 μs. A total of 12 000 and 1000 transients were acquired in 16K memories using spectral width settings of 50 kHz, acquisition times of 0.164 s, and resolution of 6.10 Hz/data point for $N(CH_3)_4^+TcO_2F_4^-$ and $TcO_2F_3{\cdot}CH_3CN$, respectively. The free induction decays were multiplied by a Gaussian function using a line broadening of −100 Hz and a Gaussian broadening factor of 0.020 prior to Fourier transformation for the $N(CH_3)_4^+TcO_2F_4^-$ sample. A line broadening of 10 Hz was used for the $TcO_2F_3{\cdot}CH_3CN$ sample. The ^{1}H (300.134 MHz) spectra were recorded at 7.0463 T using a ∼90° pulse width of 2 μs. A total of 200 transients were acquired in 16K memories using spectral width settings of 5 kHz, acquisition times of 1.638 s, resolutions of 0.61 Hz/data point, and a line broadening of 1 Hz. The ^{13}C (75.469 MHz) spectra were recorded at 7.0463 T using a ∼90° pulse width of 2 μs. A total of 10 000 transients were acquired in 16K memories using a spectral width setting of 20 kHz, an acquisition time of 0.410 s, a resolution of 2.44 Hz/data point, and a line broadening of 5 Hz. The ^{19}F, ^{99}Tc, and ^{17}O NMR spectra were referenced to external samples of neat $CFCl_3$, 0.210 M aqueous $NH_4^+TcO_4^-$, and neat H_2O, respectively, at 30 °C. The ^{1}H and ^{13}C NMR spectra were referenced to an external sample of neat TMS at 30 °C. The chemical shift convention used is that a positive (negative) sign indicates a chemical shift to high (low) frequency of the reference compound. Spin−lattice relaxation times, T_1, were measured on a Bruker AC-300 spectrometer by the standard inversion−recovery sequence using 15 variable delays ranging from 100 μs to 1 s.

Raman Spectroscopy. Raman spectra were recorded as previously described.[62] The holographic gratings used for the monochromator were 1800 grooves mm^{-1}, blazed at 550 nm for solid samples, and 1200 grooves mm^{-1}, blazed at 550 nm for liquid samples. Solid samples were recorded at room temperature in sealed in Pyrex melting point capillaries. Liquid samples were recorded at −44 °C in sealed 3-mm-o.d. Pyrex glass tubes using the macrochamber of the instrument. Low temperatures were achieved as previously described.[62] The laser power was approximately 200 mW at the sample (800 mW output power), and the monochromator slits were set to 200 μm. A total of 15 reads having 60 s integration times were summed for the Raman spectra. Depolarization measurements were obtained using the macrochamber of the instrument and method VII described by Claassen, Selig, and Shamir.[63]

Computational Methods. All calculations except for the GIAO calculations were done with the density functional theory program DGauss[64] on SGI computers. The basis set[65] for the oxygen and fluorine atoms is of the form (621/41/1) (DZVP) with a (7/3/3) fitting set. For Tc, the basis set has the form (633321/53211/531) with a fitting basis set of the form (10/5/5). For hydrogen, the basis set has the form (4/1) and a fitting basis set of the form (4). This basis set is denoted DZVP. Additional calculations were done with a slightly larger basis set of the form (7111/411/1) for oxygen and fluorine, with a (7/3/3) fitting basis set, and for technetium a (6333111/531111/5311/1) basis set was used with a fitting basis set of the form (11/6/5) (TZ94P).[66] This basis set is denoted as TZVP. The calculations were done at the local level with the potential fit of Vosko, Wilk, and Nusair[67] and at the nonlocal (gradient-corrected) level with the nonlocal exchange potential of Becke[68] combined with the nonlocal correlation functional of Perdew.[69] The geometries were optimized by using analytic gradient methods, and second derivatives were also calculated analytically.[70]

(61) Sheldrick, G. M. *SHELXTL PLUS*, Release 4.21/V; Siemens Analytical X-Ray Instruments, Inc.: Madison, WI, 1993.

(62) Casteel, W. J., Jr.; Kolb, P.; LeBlond, N.; Mercier, H. P. A.; Schrobilgen, G. J. *Inorg. Chem.* **1996**, *35*, 929.

(63) Claassen, H. H.; Selig, H.; Shamir, J. *Appl. Spectrosc.* **1969**, *23*, 8.

(64) Andzelm, J.; Wimmer, E.; Salahub, D. R. In *The Challenge of d and f Electrons: Theory and Computation*; Salahub, D. R., Zerner, M. C., Eds.; ACS Symposium Series 394; American Chemical Society: Washington, DC, 1989; p 228. Andzelm, J. In *Density Functional Theory in Chemistry*; Labanowski, J., Andzelm, J., Eds.; Springer-Verlag: New York, 1991, p 155. Andzelm, J.; Wimmer, E. *J. Chem. Phys.* **1992**, *96*, 1280. DGausss is a density functional program which is part of Unichem and is available from Oxford Molecular.

(65) Godbout, N.; Salahub, D. R.; Andzelm, J.; Wimmer, E. *Can. J. Chem.* **1992**, *70*, 560.

(66) Lee, C. Unpublished results. See: Unichem Manual, Version 3.0.

(67) Vosko, S. J.; Wilk, L.; Nusair, W. *Can. J. Phys.* **1980**, *58*, 1200.

(68) Becke, A. D. *Phys. Rev. A* **1988**, *38*, 3098. Becke, A. D. In *The Challenge of d and f Electrons: Theory and Computation*; Salahub, D. R., Zerner, M. C., Eds.; ACS Symposium Series 394; American Chemical Society: Washington, DC, 1989; p 166. Becke, A. D. *Int. J. Quantum. Chem. Symp.* **1989**, *23*, 599.

(69) Perdew, J. P. *Phys. Rev. B* **1986**, *33*, 8822.

(70) Komornicki, A.; Fitzgerald, G. *J. Chem. Phys.* **1993**, *98*, 1398 and references therein.

The NMR chemical shifts were calculated[53] at the local level with the IGLO[51] and LORG[52] approaches to treat the gauge invariance problem.

Additional NMR calculations on TcO_2F_3 and $TcO_2F_4^-$ using the GIAO approach for treating the origin problem[54] were done with the program Gaussian94 on an SGI Indigo2.[71] These calculations were done at the local level with a large basis set denoted as TZ2PF. The basis set for the NMR calculations is of triple-ζ quality[72] for oxygen and fluorine augmented by two sets of d polarization functions each formed from two Gaussian functions and an f polarization function. The technetium basis set is from Huzinga's compilation[73] and has the form (433331/43311/4211/1).

Acknowledgment. We thank the donors of the Petroleum Research Fund, administered by the American Chemical Society, for support of this work under Grant ACS-PRF No. 31198-AC3. We also thank the Natural Sciences and Engineering Research Council of Canada for the award of graduate scholarships to N.L. and the National Science Foundation (USA) for the award of a NATO Postdoctoral Fellowship to W.J.C. The density functional theory calculations were performed under the auspices of the Office of Basic Energy Sciences, U.S. Department of Energy, under Contract DE-AC06-76RLO 1830 with the Battelle Memorial Institute, which operates the Pacific Northwest National Laboratory, a multiprogram national laboratory operated for the Department of Energy. We also thank Mr. Michael Gerken for his help in obtaining the T_1 measurement for ^{99}Tc in $TcO_2F_4^-$.

Supporting Information Available: A structure determination summary (Table S11) and anisotropic thermal parameters (Table S12) (2 pages). Ordering information is given on any current masthead page.

IC9708935

(71) Frisch, M. J.; Trucks, G. W.; Schlegel, H. B.; Gill, P. M. W.; Johnson, B. G.; Robb, M. A.; Cheeseman, J. R.; Keith, T. A.; Peterson, G. A.; Montgomery, J. A.; Raghavachari, K.; Al-Laham, M. A.; Zakrzewski, V. G.; Ortiz, J. V.; Foresman, J. B.; Cioslowski, J.; Stefanov, B. B.; Nanayakkara, A.; Challacombe, M.; Peng, C. Y.; Ayala, P. Y.; Chen, W.; Wong, M. W.; Andres, J. L.; Replogle, E. S.; Gomperts, R.; Martin, R. L.; Fox, D. J.; Binkley, J. S.; Defrees, D. J.; Baker, J.; Stewart, J. J. P.; Head-Gordon, M.; Gonzalez, C.; Pople, J. A. *Gaussian 94*; Gaussian, Inc.: Pittsburgh, PA, 1995.

(72) Dunning, T., Jr. *J. Chem. Phys.* **1971**, *55*, 716.

(73) Huzinaga, S.; Andzelm, J.; Klobukowski, M.; Radzio-Andzelm, E.; Sakai, Y.; Tatewaki, H. *Gaussian Basis Sets for Molecular Calculations*; Physical Sciences Data 16; Elsevier; Amsterdam, 1984.